

RESEARCH ARTICLE

10.1002/2013WR014227

Key Points:

- Propose a connectivity-based conceptual framework of environmental response
- Present unit sedimentological responses for mud, sand, and gravel of a basin
- Resonant frequency of sediment supply leads to amplification of response

Correspondence to:

E. Foufoula-Georgiou,
efi@umn.edu

Citation:

Czuba, J. A., and E. Foufoula-Georgiou (2014), A network-based framework for identifying potential synchronizations and amplifications of sediment delivery in river basins, *Water Resour. Res.*, 50, 3826–3851, doi:10.1002/2013WR014227.

Received 4 JUNE 2013

Accepted 22 APR 2014

Accepted article online 25 APR 2014

Published online 14 MAY 2014

A network-based framework for identifying potential synchronizations and amplifications of sediment delivery in river basins

Jonathan A. Czuba¹ and Efi Foufoula-Georgiou¹

¹Department of Civil Engineering, St. Anthony Falls Laboratory, National Center for Earth-Surface Dynamics, University of Minnesota, Minneapolis, Minnesota, USA

Abstract Long-term prediction of environmental response to natural and anthropogenic disturbances in a basin becomes highly uncertain using physically based distributed models, particularly when transport time scales range from tens to thousands of years, such as for sediment. Yet, such predictions are needed as changes in one part of a basin now might adversely affect other parts of the basin in years to come. In this paper, we propose a simplified network-based predictive framework of sedimentological response in a basin, which incorporates network topology, channel characteristics, and transport-process dynamics to perform a nonlinear process-based scaling of the river-network width function to a time-response function. We develop the process-scaling formulation for transport of mud, sand, and gravel, using simplifying assumptions including neglecting long-term storage, and apply the methodology to the Minnesota River Basin. We identify a robust bimodal distribution of the sedimentological response for sand of the basin which we attribute to specific source areas, and identify a resonant frequency of sediment supply where the disturbance of one area followed by the disturbance of another area after a certain period of time, may result in amplification of the effects of sediment inputs which would be otherwise difficult to predict. We perform a sensitivity analysis to test the robustness of the proposed formulation to model parameter uncertainty and use observations of suspended sediment at several stations in the basin to diagnose the model. The proposed framework has identified an important vulnerability of the Minnesota River Basin to spatial and temporal structuring of sediment delivery.

1. Introduction

For long-term prediction of the environmental response of a basin to natural and anthropogenic disturbances, physically based distributed models are of limited use as they need many input parameters which are hard to specify and predictions become increasingly uncertain as the prediction horizon increases. For example, the transport time scale for mud (silt and clay) can be of the order of hours to days (storm-event response), while for sand and gravel can be of the order of tens to thousands of years, depending on climate and basin characteristics. When predicting such long-term response, the specific magnitude of the predicted flux might not be very accurate but the timing of the maximum flux, and also the identification of areas of the basin contributing to that maximum flux are important for long-term planning and for assessing how human-changes on a naturally evolving landscape might inadvertently affect downstream changes in many years to come.

Landscapes contain networks of dynamically connected paths (fluvial, hillslope, subsurface, etc.) that play an important role in structuring environmental fluxes and the overall basin response to a given input. An environmental response, defined as the time distribution of a quantity of interest (streamflow, sediment, nutrients, etc.) at the outlet of a basin due to a spatially distributed input, is structured by the network through time delays and transformations imposed by the physics of the environmental process operating on that network. Simplified approaches that take advantage of network topology, channel characteristics, and transport-process dynamics offer the possibility to identify hot spots or vulnerable areas/times of disturbance that can lead to synchronization and downstream amplification of the response.

Inspired by the extensive linear systems theory approach to the hydrologic response [Sherman, 1932; Nash, 1957; Dooge, 1973; Kirkby, 1976; Rodriguez-Iturbe and Valdes, 1979; Gupta et al., 1980; Troutman and Karlinger, 1985; Gupta et al., 1986; Mesa and Mifflin, 1986; Gupta and Mesa, 1988; Maidment et al., 1996; Muzik,

1996; Rinaldo *et al.*, 2006a, 2006b; Botter *et al.*, 2010] and its extension to the sedimentological response for mud at the storm-event time scale [Johnson, 1943; Williams, 1978; Kumar and Rastogi, 1987; Sharma *et al.*, 1992; Raghuvanshi *et al.*, 1994; Gracia-Sanchez, 1996; Lee and Singh, 1999; Kalin *et al.*, 2004a, 2004b; Singh *et al.*, 2008; Bhunya *et al.*, 2010; Lee and Yang, 2010], we propose here a conceptual framework for computing the “sedimentological response function” of a basin focusing specifically on the transport of mud, sand, and gravel. The sedimentological response function is defined as the time distribution of the sediment quantity delivered to the outlet of a basin in response to an instantaneous unit input of sediment uniformly distributed over the basin. This response function is computed by performing a nonlinear process-based scaling of the network width function (the probability distribution of distances to the outlet) into a time response function. The framework incorporates not only the network topology but also (via process-based scaling) specific attributes of the three-dimensional structure of the landscape, stream morphology, and hydrodynamics that contribute to sediment production and transport, such as slope, depth, and width of the river at any location, shear stress of the bed, relevant magnitude/frequency of flow, etc. Using scaling functions (such as hydraulic geometry), the proposed framework can be considerably simplified and reduced down to a few parameters that can convert the network width function to a process-scaled response function.

In this paper, we present the proposed framework for transport of mud, sand, and gravel and demonstrate it in a specific high sediment production regime in the Minnesota River Basin. This basin was selected as a prototype because excessive sediment impairs river water quality and biotic functioning, and the management of current and future actions on the landscape requires unraveling the temporal and spatial effects of these actions, as well as understanding how the environment continues to respond to past actions and disturbances.

2. Conceptual Framework of Environmental Response

The proposed connectivity-based conceptual framework of environmental response relies on performing a physically based scaling of the distances (link lengths) along the network by characteristic velocities of the flux transported on the network to obtain the “environmental response function” for the flux of interest. The environmental response function provides significant insight into the “workings of the system” (in terms of both its structural components and dynamics) and provides a building block for computing the flux at the outlet of the basin in response to any temporally variable input in the basin, under of course, the proportionality and superposition assumptions of linear system theory. The theoretical basis of the proposed framework rests on the link between Lagrangian and Eulerian transport formalisms by which one can establish the relation between the evolution in time and space of the trajectories of an ensemble of particles injected over a set of points at an initial time and transported over all possible trajectories in the network, to the first passage (or travel time) distribution at a fixed control section, here at the outlet of the basin [e.g., Rodriguez-Iturbe and Rinaldo, 1997].

Let the river network be defined by a set of hierarchically connected links i , where a link is defined as the segment of the network between a source and a junction (a source link), two successive junctions, or a junction and the basin outlet. Junctions are the points at which two links join, sources are the points farthest upstream in the network, and the outlet is the point farthest downstream in the network. Each link i is assigned a geomorphic fluvial state $\xi_{f,i}$ which may include geomorphologic and hydraulic attributes of the link, i.e., $\xi_{f,i}(\ell_i, a_i, A_i, S_i, Q_{w,i}, H_i, B_i, \dots)$, where the geomorphologic attributes may include the link length ℓ_i [L], directly contributing area a_i [L²], upstream drainage area A_i [L²], and link slope S_i , and the hydraulic attributes may include the streamflow $Q_{w,i}$ [L³ T⁻¹], cross-section average depth H_i [L], average width B_i [L], etc. (Figure 1a). While not indicated explicitly, attributes of the geomorphic state $\xi_{f,i}$ may also be a function of time to capture possible time-varying properties of the system.

Let now γ_i denote the pathway (set of links) that a particle initiating at link i will follow along the river network to reach the outlet. The properties of this pathway are defined by the hierarchical (directed) collection of the geomorphic fluvial states of the links composing γ_i , i.e., $\{\xi_i, \dots, \xi_\Omega\}$ from the geomorphic state ξ_i through the network to the outlet (i.e., $\xi_i \rightarrow \dots \rightarrow \xi_\Omega$). It is noted that, in general, a landscape can be seen as a set of connected paths, which in addition to fluvial paths might include hillslope, subsurface, floodplain, pond/wetland, pipe, etc., paths which can also be incorporated in the above framework if their properties are known. In what follows we restrict ourselves to fluvial paths only.

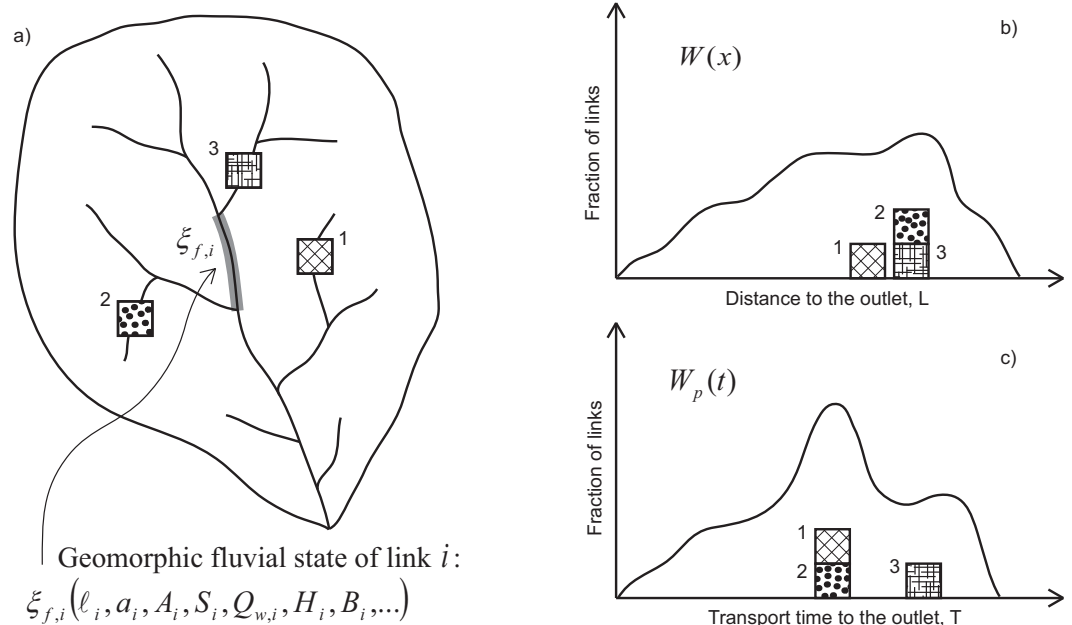


Figure 1. Conceptual framework of environmental response. (a) Illustration of a river basin with fluvial channel network. The highlighted segment of the network is a link i corresponding to geomorphic fluvial state $\xi_{f,i}$ with associated attributes. Areas of the basin, such as 1, 2, and 3, sitting at a certain distance from the outlet contribute to (b) a specific structure of the width function $W(x)$. (c) The contribution of these areas to the outlet may be redistributed in the process-scaled width function $W_p(t)$ based on the characteristics of the process of interest. The resulting environmental response function is a complex transformation of the original width function that depends on the river network topology and the attributes of the geomorphic fluvial states $\xi_{f,i}$ for all i links.

A particle introduced into link i has a pathway distance L_i [L] from that point to the outlet given by

$$L_i = \sum_{j \in \gamma_i} \ell_j, \tag{1}$$

which is the sum of link lengths along pathway γ_i . The width function (WF) $W(x)$ is defined as the number of links in the network (typically normalized by the total number of links) which are found at a discretized pathway distance x [L] from the outlet measured along the network (Figure 1b). Thus, in the limit of a large number of pathways, the WF is the probability distribution of pathway distances to the outlet of the basin. The directed network of link lengths ℓ_i [L] may be transformed to a directed network of travel times $t_{p,i}$ [T] based on a process operating on the network, say through a process-specific velocity $u_{p,i}$ [$L T^{-1}$] of the transported environmental flux. The travel time $t_{p,i}$ is the time it takes a particle to move through (or the time during which a particle is in) geomorphic state ξ_i and is given by

$$t_{p,i} = \frac{\ell_i}{u_{p,i}}. \tag{2}$$

Note that $t_{p,i}$ must include both the time when the particle is actually moving and the time when it is not being transported, i.e., it stays in storage within link i . When long-term storage is present, then $u_{p,i}$ represents a virtual velocity whose physical meaning has to be interpreted with caution. Here as detailed in section 3, long-term storage effects are ignored and only short-term storage (due to the intermittency of flood events capable of transporting sediment) is incorporated via an intermittency factor formalism (explained in more detail in Appendix B). Considering this length-to-time conversion, a particle introduced into link i has a pathway travel time $T_{p,i}$ [T] to the outlet given by

$$T_{p,i} = \sum_{j \in \gamma_i} t_{p,j}, \tag{3}$$

which is the sum of travel times along pathway γ_i . Thus, when such transport dynamics are introduced on the river network, each pathway distance to the outlet is scaled to a travel time to the outlet. This allows one to compute the probability that a particle found at the outlet at time t [T] was in position x (and thus

within an upstream link at distance x from the outlet) at time $t = 0$. This distribution produces a process-scaled width function (PSWF) $W_p(t)$ defined as the number of links in the network (normalized by the total number of links) that contribute to the outlet at time t (Figure 1c). This PSWF is also the probability distribution of pathway travel times of particles (introduced instantaneously and uniformly in all links in the network) to the outlet of the basin, and as such relates to the geomorphologic instantaneous unit response function (GIURF) of the basin. It is understood that the contributions of different areas of the basin to the WF may be considerably redistributed in the PSWF based on the characteristics of the process of interest (Figure 1); e.g., particles injected at two points which are at the same distance to the outlet might arrive at the outlet at significantly different times depending on the transport properties of their pathways (slopes, channel hydraulic properties, bed friction, etc.). Obviously, if the process-specific velocity u_p is constant for all links, the PSWF (normalized by the maximum process-specific pathway travel time $T_{p,max}$ [T]) and the WF (normalized by the maximum pathway distance L_{max} [L]) coincide. In section 3, the PSWF (or GIURF) is formulated for mud, sand, and gravel transport in a river network.

3. Formulation of the Sedimentological Response Function

Sediment in large and small quantities is intermittently and spatially nonuniformly supplied to river networks [Benda and Dunne, 1997a, 1997b; Reid et al., 2007a] across a broad range of sizes that include clay (<4 μm), silt (4–62 μm), sand (0.062–2 mm), gravel (2–64 mm), and cobbles (6.4–25.6 cm) (following the sedimentological phi scale of Garcia [2008]). Once emplaced in the river, sediment is transported downstream by the next capable streamflow and transitions between various transient storage zones (e.g., channel bed, bars, floodplain) on its way to the outlet [Harvey, 2002; Malmon et al., 2003; Reid et al., 2007b; Lauer and Parker, 2008; Fryirs, 2013; Pizzuto et al., 2014].

The connectivity-based conceptual framework of environmental response is applied to the process of sediment transport. Herein, equations for the characteristic velocity of sediment are developed for mud (within a particle-size range for clay and silt), sand, and gravel (a term used herein to collectively describe the particle-size range for gravel and cobbles) considering only the transport time (and not long-term storage time) through each geomorphic fluvial state $\xi_{f,i}$. In many systems, storage is an important component in the transfer of sediment out of a basin and must be incorporated in sediment-transport formulations. In principle, there is no conceptual difficulty in incorporating storage in the sedimentological response function approach presented here, by specifying residence times and accounting for the transitions between the channel and transient storage zones (e.g., floodplains); however, lack of data for its characterization has prompted us to exclude it from the present analysis. The equations for the characteristic velocity for each class of sediment (developed under a set of clearly defined assumptions) are used to develop PSWFs, which represent the geomorphologic instantaneous unit sedimentographs (GIUS) for each class of sediment. It is noted that for any real system subject to temporally variable inputs, the observed response at the outlet can be realized by convolving partitioned and scaled versions of the GIUS that reflect the specific sediment supply conditions. Also, spatially variable inputs can be handled by computing the GIUS over smaller basins where sediment input can be comfortably considered spatially uniform.

3.1. Mud Response Function

During transport by streamflow, turbulence is generally strong enough to carry mud (clay and silt) in continuous suspension. This leads to a uniform distribution of mud in the water column, a characteristic vertical length scale for mud transport as the flow depth, and a characteristic velocity of mud transport as that of the streamflow.

The characteristic velocity of mud transport (streamflow velocity) $u_{w,i}$ [$L T^{-1}$] can be obtained in several ways, including through hydraulic equations and hydraulic geometry relations. However, hydraulic equations, such as Manning's equation, require the specification of a channel roughness in addition to a characteristic streamflow throughout the network. The specified channel roughness should be verified against hydraulic measurements to ensure the simulated hydraulics is reasonable and not driving the flow toward supercritical on moderate slopes. Hydraulic geometry relations specify hydraulic variables based on a characteristic streamflow or drainage area alone, and these relations can be readily determined from gage data within the basin. Using hydraulic geometry, the characteristic velocity of mud transport (streamflow) scales as

$$u_{w,i} = \alpha_{u_w A} A_i^{\beta_{u_w A}} \tag{4}$$

where $A_i [L^2]$ is the drainage area upstream of the i th link, and $\alpha_{u_w A}$ and $\beta_{u_w A}$ are the coefficient and exponent, respectively, of the scaling relation. The parameters $\alpha_{u_w A}$ and $\beta_{u_w A}$ can be determined directly from gage data within the basin or in the absence of these data, typical hydraulic geometry exponents can be used [Leopold and Maddock, 1953; Leopold et al., 1964; Park, 1977]. The characteristic velocity scaling of equation (4) leads to the travel time scaling as

$$t_{w,i} = \frac{\ell_i}{\alpha_{u_w A}} A_i^{-\beta_{u_w A}}. \tag{5}$$

Summing the travel time along pathway γ_i gives the pathway travel time as

$$T_{w,i} = \sum_{j \in \gamma_i} t_{w,j}, \tag{6}$$

which can be used to obtain the PSWF for mud transport (streamflow) $W_w(t)$.

3.2. Sand Response Function

Sand is transported by streamflow throughout the water column, with the highest concentrations near the bed. Turbulence acts to lift sand into suspension; the weight of particles cause it to fall back toward the bed. In the absence of sufficient turbulence to lift sand into suspension, sand is transported along the bed. The characteristic velocity of sand can be described as a bulk velocity of sand $u_{s,i} [L T^{-1}]$ and can be obtained by combining equations for the volumetric transport rate of sand, channel hydraulics, and sand transport.

The volumetric transport rate of sand $Q_{s,i} [L^3 T^{-1}]$ can be decomposed as

$$Q_{s,i} = u_{s,i} (\theta_i H_i) B_i, \tag{7}$$

where $H_i [L]$ is the channel depth, θ_i is a scale factor, and $B_i [L]$ is the channel width of the i th link. The term $\theta_i H_i$ defines a characteristic vertical length scale for sand transport where the majority of sand transport takes place. The scale factor θ_i will vary depending on the flow (turbulence): larger for higher flows when more sand is lifted into suspension and smaller for lower flows when sand primarily transports along the bed.

Streamflow exerts a stress on the sediment composing the bed, which can be estimated assuming uniform (normal) flow for the channel hydraulics as

$$\tau_{b,i} = \rho g H_i S_i = \rho C_{f,i} u_{w,i}^2, \tag{8}$$

where $\tau_{b,i} [M L^{-1} T^{-2}]$ is the bed shear stress, S_i is the channel slope, and $C_{f,i}$ is the friction coefficient of the i th link, ρ is the density of water $[M L^{-3}]$, and g is the acceleration due to gravity $[L T^{-2}]$. Additionally, the volumetric transport rate of water $Q_{w,i} [L^3 T^{-1}]$ through the i th link is

$$Q_{w,i} = u_{w,i} H_i B_i. \tag{9}$$

The stress exerted on the bed sediment can be related to the transport rate of that sediment through the sand-transport formula of Engelund and Hansen [1967] for the total sand load (neglecting the shear stress partition for bed forms) as

$$q_{s*,i} = \frac{0.05}{C_{f,i}} (\tau_{*,i})^{5/2}, \tag{10}$$

where $q_{s*,i}$ is the dimensionless volumetric transport rate of sand per unit width and $\tau_{*,i}$ is the dimensionless bed shear stress in the i th link,

$$q_{s*,i} = \frac{q_{s,i}}{\sqrt{R_i g D_i D_i}}, \quad (11)$$

where $q_{s,i}$ [$L^2 T^{-1}$] is the volumetric transport rate of sand per unit width, R_i is the submerged specific gravity of sediment, and D_i [L] is the sediment grain size in the i th link,

$$q_{s,i} = \frac{Q_{s,i}}{B_i}, \quad (12)$$

and

$$\tau_{*,i} = \frac{\tau_{b,i}}{\rho g R_i D_i}. \quad (13)$$

The above equations relate streamflow to bed shear stress to sand-transport rate to the characteristic velocity of sand transport. These equations combine and simplify to

$$u_{s,i} = \frac{0.05}{\theta_i g^{1/2} R_i^2 D_i} u_{w,i}^2 H_i^{1/2} S_i^{3/2}. \quad (14)$$

As mentioned above, there are several ways of obtaining relations for flow velocity and depth. Again, hydraulic geometry relations are used to provide equations for flow velocity from equation (4) and depth as

$$H_i = \alpha_{HA} A_i^{\beta_{HA}}, \quad (15)$$

where α_{HA} and β_{HA} are the coefficient and exponent, respectively, of the scaling relation. The parameters α_{HA} and β_{HA} can be determined directly from gage data within the basin or in the absence of these data, typical hydraulic geometry exponents can be used [Leopold and Maddock, 1953; Leopold et al., 1964; Park, 1977].

Substituting the relations for the flow velocity (equation (4)) and depth (equation (15)) into equation (14) provides an equation for the characteristic velocity of sand transport in terms of variables that can be specified or easily extracted from a digital elevation model (DEM) as

$$u_{s,i} = \frac{0.05}{\theta_i g^{1/2} R_i^2 D_i} \alpha_{u_w A}^2 \alpha_{HA}^{1/2} A_i^{2\beta_{u_w A} + \beta_{HA}/2} S_i^{3/2}. \quad (16)$$

The characteristic velocity scaling of equation (16) leads to a travel time scaling of

$$t'_{s,i} = \frac{\theta_i g^{1/2} R_i^2 D_i}{0.05 \alpha_{u_w A}^2 \alpha_{HA}^{1/2}} \ell_i A_i^{-(2\beta_{u_w A} + \beta_{HA}/2)} S_i^{-3/2}, \quad (17)$$

where $t'_{s,i}$ is the travel time of sand in geomorphic fluvial state $\zeta_{f,i}$, and in this formulation, a characteristic flow is implicitly tied to the scaling of hydraulic variables with drainage area. Therefore, $t'_{s,i}$ represents the time it would take sand to move through geomorphic fluvial state $\zeta_{f,i}$ if the flow implicit in the hydraulic scaling were held constant during this time.

However, streamflows capable of significantly transporting sediment occur for short periods intermittently throughout the year. As a simplification, rather than determining incremental travel times for sediment based on daily flows, a representative flow that transports sediment, such as bankfull flow, can be used to determine the channel hydraulics. Then a simulated time of continuous bankfull flow can be translated into real time by incorporating an intermittency factor $I_{f,s}$ [Paola et al., 1992; Parker, 2004] where

$$t'_{s,i} = I_{f,s} t_{s,i}. \quad (18)$$

The intermittency factor denotes the fraction of time per year that continuous bankfull flow would yield the mean annual sand load. In this way, time is scaled so that in 1 year, the mean annual sand load has been

transported by continuous bankfull flow. It is important to note that the intermittency factor is specified with respect to the sand-transport process and not (directly) from the recurrence of the bankfull flow.

Introducing the intermittency factor of equation (18) into equation (17) leads to the travel time scaling of

$$t_{s,i} = \frac{\theta_i g^{1/2} R_i^2 D_i}{0.05 \alpha_{u_w A}^2 \alpha_{HA}^{1/2} I_{f,s}} \ell_i A_i^{-(2\beta_{u_w A} + \beta_{HA}/2)} S_i^{-3/2}. \quad (19)$$

Summing the travel time along pathway γ_i gives the pathway travel time

$$T_{s,i} = \sum_{j \in \gamma_i} t_{s,j}, \quad (20)$$

which can be used to obtain the PSWF for sand transport $W_s(t)$.

3.3. Gravel Response Function

Gravel (gravel and cobbles) is much larger in size than sand and is therefore much harder to move. Thus, gravel is transported by streamflow along the bed of a river. The transport of gravel occurs in a layer of active transport that is typically a few particle diameters thick [Parker, 2008]. The development of the characteristic velocity of gravel $u_{g,i}$ [$L T^{-1}$] is similar to that for sand, but specific to gravel transport, which includes an appropriate characteristic vertical length scale and sediment-transport relation for gravel transport. The equations for channel hydraulics for uniform (normal) flow remain the same.

The volumetric transport rate of gravel $Q_{g,i}$ [$L^3 T^{-1}$] can be decomposed as

$$Q_{g,i} = u_{g,i} L_{a,i} B_i, \quad (21)$$

where $L_{a,i}$ [L] is the active layer thickness of the i th link and defines a characteristic vertical length scale for gravel transport. The stress exerted on the bed sediment can be related to the transport rate of that sediment through a gravel-transport formula [e.g., Wong and Parker, 2006] of the form

$$q_{g*,i} = \alpha_g (\tau_{*,i} - \tau_{*,c,i})^{\beta_g}, \quad (22)$$

where $q_{g*,i}$ is the dimensionless volumetric transport rate of gravel per unit width and $\tau_{*,c,i}$ is the critical dimensionless bed shear stress for the initiation of motion in the i th link, α_g and β_g are the coefficient and exponent of the gravel-transport formula, respectively,

$$q_{g*,i} = \frac{q_{g,i}}{\sqrt{R_i g D_i D_i}}, \quad (23)$$

where $q_{g,i}$ [$L^2 T^{-1}$] is the volumetric transport rate of gravel per unit width and

$$q_{g,i} = \frac{Q_{g,i}}{B_i}. \quad (24)$$

The above equations relate streamflow to bed shear stress to gravel transport rate to the characteristic velocity of gravel transport. These equations combine and simplify to

$$u_{g,i} = \frac{R_i^{1/2} g^{1/2} D_i^{3/2} \alpha_g}{L_{a,i}} \left(\frac{H_i S_i}{R_i D_i} - \tau_{*,c,i} \right)^{\beta_g}. \quad (25)$$

Substituting the scaling relation for flow depth (equation (15)) into equation (25) provides an equation for the characteristic velocity of gravel transport in terms of variables that can be specified or easily extracted from a DEM as

$$u_{g,i} = \frac{R_i^{1/2} g^{1/2} D_i^{3/2} \alpha_g}{L_{a,i}} \left(\frac{\alpha_{HA} A_i^{\beta_{HA}} S_i}{R_i D_i} - \tau_{*c,i} \right)^{\beta_g} \quad (26)$$

The characteristic velocity scaling of equation (26) leads to a travel time scaling of

$$t'_{g,i} = \frac{L_{a,i}}{R_i^{1/2} g^{1/2} D_i^{3/2} \alpha_g} \ell_i \left(\frac{\alpha_{HA} A_i^{\beta_{HA}} S_i}{R_i D_i} - \tau_{*c,i} \right)^{-\beta_g}, \quad (27)$$

where $t'_{g,i}$ is the travel time of gravel in geomorphic fluvial state $\xi_{f,i}$, and in this formulation, a characteristic flow is implicitly tied to the scaling of hydraulic variables with drainage area. As for sand, bankfull flow is used to determine the scaling of the channel hydraulics. Therefore, a simulated time of continuous bankfull flow can be translated into real time by incorporating an intermittency factor $I_{f,g}$ [Paola et al., 1992; Parker, 2004] where

$$t'_{g,i} = I_{f,g} t_{g,i}. \quad (28)$$

The intermittency factor denotes the fraction of time per year that continuous bankfull flow would yield the mean annual gravel load. The intermittency factor for gravel transport is different from the intermittency factor for sand even though the streamflow driving the process may be the same. Introducing the intermittency factor of equation (28) into equation (27) leads to the travel time scaling of

$$t_{g,i} = \frac{L_{a,i}}{R_i^{1/2} g^{1/2} D_i^{3/2} \alpha_g I_{f,g}} \ell_i \left(\frac{\alpha_{HA} A_i^{\beta_{HA}} S_i}{R_i D_i} - \tau_{*c,i} \right)^{-\beta_g}. \quad (29)$$

Summing the travel time along pathway γ_i gives the pathway travel time

$$T_{g,i} = \sum_{j \in \gamma_i} t_{g,j}, \quad (30)$$

which can be used to obtain the PSWF for gravel transport $W_g(t)$.

3.4. Major Assumptions

The GIUS is the sedimentological response of a basin to the generation of an instantaneous unit volume of sediment uniformly entering all links of the network; it explicitly incorporates the network topology, channel characteristics, and transport-process dynamics. The PSWF for mud, sand, and gravel (developed herein) is the GIUS for each class of sediment under the following assumptions:

1. Uniform (normal) flow.
2. Wide rectangular channel; that is, the hydraulic radius is approximated by the average depth.
3. The scaling of hydraulic characteristics (streamflow, velocity, depth, and width) from gages represents the hydraulics of the entire channel network.
4. The bankfull flow is constant during the entire period of response. The sedimentological effect (for sand and gravel) from a simulated bankfull flow can be transformed into real time by an intermittency factor.
5. Sediment-transport formulas (of the form of Engelund and Hansen [1967] for sand and Wong and Parker [2006] for gravel) represent the sediment-transport process.
6. Total shear stress drives sediment transport. There is no partitioning of shear stress due to the potential presence of bed forms.
7. The characteristic velocity of sediment can be obtained from the volumetric transport rate of sediment divided by a characteristic area (channel width B , multiplied by a characteristic vertical length scale, H_i for mud, $\theta_i H_i$ for sand, and $L_{a,j}$ for gravel).
8. No storage or morphologic change occurs in the river network over time. That is, there is no erosion, deposition, or change in any channel characteristics over time; there is no feedback from sediment transport back to channel morphology. The sediment supplied does not overwhelm the transport capacity.

9. No mechanism is present for dispersion of sediment other than geomorphologic dispersion due to the network topology.
10. No attrition of sediment occurs within the river network. That is, the sediment supplied to the system retains its size through the system. Sediment does not abrade or break down into smaller particles as it is transported downstream.
11. Delivery of sediment to the network is represented by an instantaneous unit input of sediment with grain size D , supplied to the upstream end of links.
12. Every point in the watershed drains to a singular, unique outlet point. No local depressions are allowed in the network; only geomorphic fluvial states.
13. Sedimentological response is linear. Individual responses can be superimposed with each other.
14. Sedimentological response is time invariant. The response is always the same irrespective of when it occurs.

This paper explores a formulation of the GIUS for mud, sand, and gravel and as a first step toward understanding basin-scale response of sediment, it makes several simplifying assumptions as discussed above. However, many of these assumptions can be relaxed within the proposed framework to provide a more realistic sedimentological response.

4. Application to the Minnesota River Basin

The Minnesota River accounts for 80–90% of the total sediment delivered to Lake Pepin, a naturally dammed lake on the Mississippi River about 80 km downstream of the mouth of the Minnesota River (Figure 2), from the combined basins of the Minnesota, St. Croix, and upper Mississippi Rivers, despite the fact that it accounts for only about one third of the total drainage area [Kelley and Nater, 2000]. The Minnesota River drains approximately 44,000 km² in southern Minnesota and parts of South Dakota, Iowa, and North Dakota, and is tributary to the Mississippi River just south of Minneapolis-St. Paul, Minnesota (Figure 2). The landscape of the Minnesota River Basin has been sculpted by glaciers and geomorphic processes associated with their retreat, notably with the carving of the Minnesota River valley after glacial Lake Agassiz drained catastrophically through the proto-Minnesota River 13,400 years ago [Clayton and Moran, 1982]. The incision of the main stem Minnesota River reduced the base level of its tributaries which created knick-points, or sharp increases in channel gradient, at the mouths of tributaries. Over time the knickpoints have migrated upstream creating knick-zones of rapidly incising channels, disconnected from their floodplains, with steep slopes that actively erode bluffs and ravines [Gran et al., 2009, 2011; Belmont, 2011; Belmont et al., 2011]. Streams meander

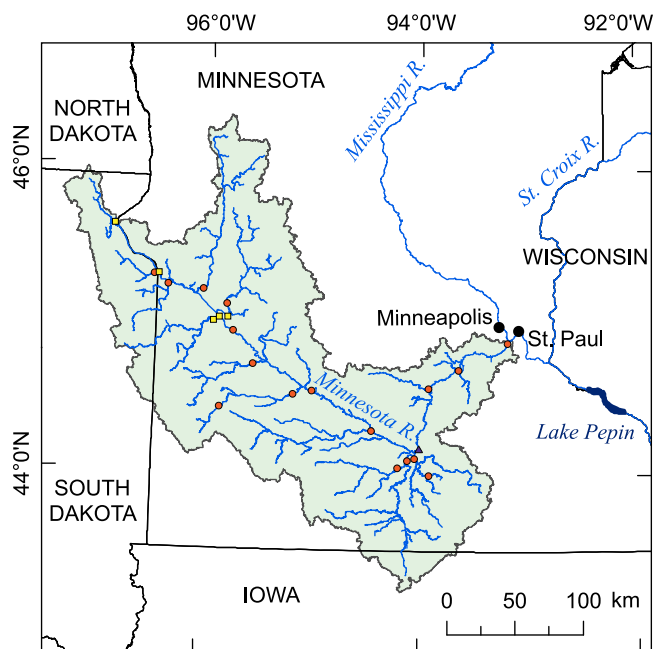


Figure 2. Location map of the Minnesota River Basin. 23 U.S. Geological Survey (USGS) streamflow-gaging stations (red circles, yellow squares, and purple triangle) used in the hydraulic geometry scaling analysis (see Appendix A), USGS streamflow-gaging station 05325000, Minnesota River at Mankato, Minnesota (purple triangle) used in estimating the intermittency factor for sand transport (see Appendix B), and 18 USGS streamflow-gaging stations (red circles and purple triangle) used in estimating the rate of total sand transport from suspended-sediment measurements (see Appendix C).

River drains approximately 44,000 km² in southern Minnesota and parts of South Dakota, Iowa, and North Dakota, and is tributary to the Mississippi River just south of Minneapolis-St. Paul, Minnesota (Figure 2). The landscape of the Minnesota River Basin has been sculpted by glaciers and geomorphic processes associated with their retreat, notably with the carving of the Minnesota River valley after glacial Lake Agassiz drained catastrophically through the proto-Minnesota River 13,400 years ago [Clayton and Moran, 1982]. The incision of the main stem Minnesota River reduced the base level of its tributaries which created knick-points, or sharp increases in channel gradient, at the mouths of tributaries. Over time the knickpoints have migrated upstream creating knick-zones of rapidly incising channels, disconnected from their floodplains, with steep slopes that actively erode bluffs and ravines [Gran et al., 2009, 2011; Belmont, 2011; Belmont et al., 2011]. Streams meander

through low-gradient uplands above the knickzones, and are tributary to the low-gradient, meandering, main stem Minnesota River downstream of the knickzones.

Around the time of European settlement in the mid-1800s, the Minnesota River Basin was dominated by tall-grass prairie and dotted with poorly drained wetlands [Marschner, 1974]. Beginning in the late 1800s, surface ditches were dug and subsurface drainage tiles were installed to drain wetlands and uplands for agriculture. As of 2007, agriculture accounted for around 90% of land-use in the basin [Musser et al., 2009]. Wetlands that were once connected by subsurface flow paths to the Minnesota River are now connected to the river by a vast network of drainage tiles and ditches, which has greatly changed the hydrologic connectivity of the basin and the rate at which water enters the river after rainfall. Late 19th century and early 20th century agricultural practices largely disturbed the landscape and increased sediment loads to the river network, initially by top-soil erosion. As soil-conservation practices improved and underground tile drainage expanded, sources of sediment shifted from upland fields to river banks and bluffs caused by increased streamflow due the combined effects of increased precipitation, crop conversions, and primarily amplified runoff from agricultural tile drainage [Belmont et al., 2011; Schottler et al., 2014].

4.1. Extraction of Network and Link Attributes and Spatial Heterogeneity of the Basin

A 30 m DEM was downloaded in tiles covering the entire Minnesota River Basin from the U.S. Geological Survey (USGS) National Map with a coordinate system in the North American Datum of 1983 (NAD83) in decimal degrees and North American Vertical Datum of 1988 (NAVD88) in meters [U.S. Geological Survey, 2012]. Using ArcGIS, the tiles were mosaicked and projected into the Universal Transverse Mercator zone 15N (UTM15N) coordinate system. A drainage network was extracted for the Minnesota River Basin using ArcHydro tools in ArcGIS and a threshold area of 10 km². Although this threshold area is too large to extract all fluvial channels in the river network, the extracted network sufficiently captures the major fluvial channels and for simplicity, ignores the lowest order drainage ditches, whose initiation may not be based on a

simple threshold area [Passalacqua et al., 2012]. This produced a network of links each with attributes: index of link *i*, index of upstream link, index of downstream link, link length ℓ_i , directly contributing area a_i , and upstream drainage area A_i .

The elevation at the upstream and downstream end of each link was extracted from the underlying DEM, differenced, and divided by link length (channel path length) to determine the slope *S_i* of each link (Figure 3). The elevations extracted from the DEM for the river network represent the water surface and not the riverbed. The slope of the water surface is equivalent to the slope of the riverbed under uniform flow conditions which is likely approximate for most of the network. However, around tributaries where there is backwater, the uniform flow assumption is violated, the slope of water surface is less than the slope of the riverbed, and the slopes obtained from elevations extracted from the DEM likely underestimate the slope of the riverbed. To account for this, specifically in the lower main stem Minnesota River, all slopes less than 0.0001 were

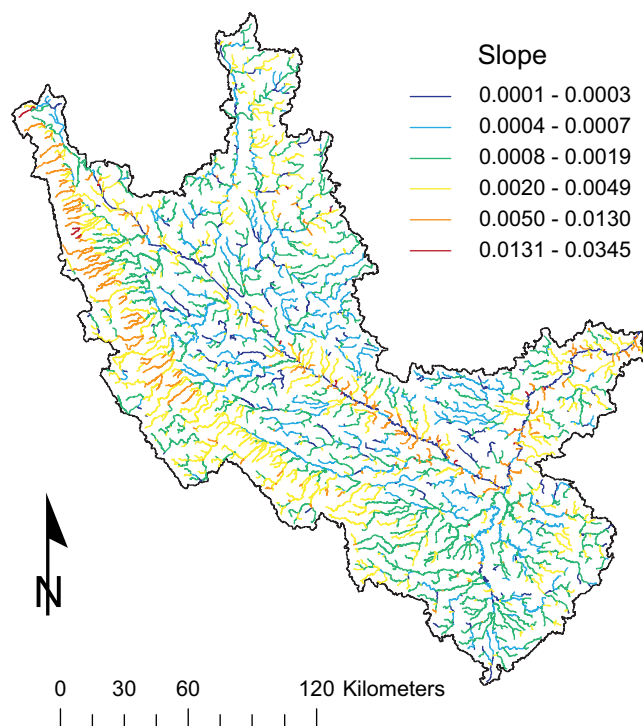


Figure 3. Slope of each link in the network. Highest slopes occur in the knickzones of tributaries entering the main stem Minnesota River and in the north-western part of the basin. Note that slopes less than 0.0001 were set to this value; this occurred primarily along the lower main stem Minnesota River. The spatial distribution of link slopes vividly illustrates the geologic legacy of this basin with important implications for spatially variable sediment generation and transport.

set to this value. However, if the adjusted slopes are actually much less than this value, then the simulated transport time through these links will be much faster than the actual transport time. For the Minnesota River Basin, the highest slopes in the network occur in the knickzones of tributaries entering the main stem Minnesota River and in the northwestern part of the basin; between these regions are low-gradient uplands (Figure 3). The heterogeneity of slopes within the basin leads to nonuniform transport velocities, supporting the need for a spatially explicit analysis of process response. Finally, all attributes were exported from ArcGIS and imported into MatLab for computing the sedimentological response.

4.2. Formulation of Travel Times

In this section, parameters of the sedimentological response function for mud, sand, and gravel (developed in section 3) are specified based on characteristics of the Minnesota River Basin.

4.2.1. Mud Response Function

Hydraulic geometry scaling relations for the Minnesota River Basin were developed at an approximate bankfull flow chosen as the 2 year recurrence interval peak flow Q_2 or 2 year flow (Appendix A) from which estimates were obtained for the parameters $\alpha_{u_wA} = 0.20$, and $\beta_{u_wA} = 0.07$ for the streamflow velocity scaling equation (4), and thus the characteristic velocity of mud transport, as

$$u_{w,i} = (0.20)A_i^{0.07}, \tag{31}$$

where A_i is specified in m^2 and $u_{w,i}$ in m/s .

The characteristic velocity scaling of equation (31) leads to the travel time scaling of

$$t_{w,i} = 5\ell_i A_i^{-0.07}, \tag{32}$$

where ℓ_i is specified in meters and thus $t_{w,i}$ in seconds. Summing the travel time along each pathway γ_i gives the pathway travel time $T_{w,i}$, which can be used to obtain the PSWF for mud transport (streamflow) $W_w(t)$.

4.2.2. Sand Response Function

The characteristic velocity of sand for the Minnesota River Basin was obtained by substituting the parameters $g = 9.81 \text{ m s}^{-2}$, $\theta_i = 0.1$ ($\forall i$), $R_i = 1.65$ ($\forall i$), $D_i = 0.0004 \text{ m}$ ($\forall i$; D50 size of sand from riverbed material within the Minnesota River Basin [U.S. Geological Survey, 2013]), $\alpha_{u_wA} = 0.20$, $\beta_{u_wA} = 0.07$, $\alpha_{HA} = 0.0029$, and $\beta_{HA} = 0.29$ (Appendix A; at Q_2 or 2 year flow, where A_i is specified in m^2 , H_i in m , and $u_{w,i}$ in m/s) into equation (16), which reduces the characteristic velocity of sand to

$$u_{s,i} = 0.32A_i^{0.285}S_i^{3/2}, \tag{33}$$

where $u_{s,i}$ is specified in m/s . Substituting the intermittency factor $I_{f,s} = 0.175$ (Appendix B) into equation (19) and incorporating equation (33) leads to the travel time scaling of

$$t_{s,i} = 18\ell_i A_i^{-0.285}S_i^{-3/2}, \tag{34}$$

where again ℓ_i is specified in meters and thus $t_{s,i}$ in seconds. Summing the travel time along each pathway γ_i gives the pathway travel time $T_{s,i}$, which can be used to obtain the PSWF for sand transport $W_s(t)$.

4.2.3. Gravel Response Function

The gravel transport equation contains a threshold for transport (see equations (22) and (29)); above the threshold, transport occurs and below the threshold no transport occurs. The flow is capable of transporting gravel when the dimensionless bed shear stress

$$\tau_{*,i} = \frac{H_i S_i}{R_i D_i} \tag{35}$$

exceeds the threshold value for initiation of motion $\tau_{*,i} > \tau_{*c,i}$, where $\tau_{*c,i} = 0.0495$ for the Wong and Parker [2006] gravel-transport formula. The proposed formulation for gravel response only exists if the transport

threshold is exceeded everywhere in the basin (otherwise contributions from the basin can never be transported to the outlet). Therefore, the flow is capable of transporting gravel when, and the GIUS for gravel for the Minnesota River Basin only exists if,

$$S_i > \frac{\tau_{*c,i} R_i D_i}{\alpha_{HA}} A_i^{-\beta_{HA}} \quad (36)$$

for the Q_2 . Considering the potential transport of sediment with a grain size of $D_i = 0.01$ m ($\forall i$; and the other parameters specified based on those given for the sand response function), the transport threshold is not exceeded everywhere in the basin for this formulation, and therefore, the gravel response function does not exist at the outlet of the basin at the Q_2 . This suggests that this size gravel is not transported out of the Minnesota River Basin at or below the Q_2 . For this reason, we do not go into further details about the gravel response and leave further investigations that consider spatially variable grain size, abrasion, and variable flow above the Q_2 , for a future study.

However, mapping where the river system is capable of transporting gravel ($\tau_{*,i} - \tau_{*c,i} > 0$) would provide insight into potential transport and deposition areas of the network. While this map is not shown, the areas where the river system is capable of transporting gravel are those with the steepest slopes (Figure 3) in the knickzones of tributaries entering the main stem Minnesota River and in the northwestern part of the basin. Gravel supplied to channels capable of transporting this material will eventually be transported downstream (and abrade or break down into smaller particles) until it reaches a channel that is not capable of transporting this material. These downstream channels are potential deposition reaches for gravel as any gravel supplied to it would accumulate at this location. Additionally, channels capable of transporting gravel are those with the greatest capacity for erosion and these channels may indicate potential sediment sources where the river is capable of recruiting bank material into the channel.

5. GIUS of the Minnesota River Basin

The proposed formulation of the GIUS describes how sediment with grain size D_i instantaneously released and uniformly distributed over the basin would propagate (below transport capacity) through the river system to the basin outlet. We repeat that the present formulation only considers storage (time delays) for sediment on the bed or on bars that are readily mobilized by the next capable flow. Long-term storage of sediment due to floodplain deposition or meander migration over a bar that is re-entrained when the river sweeps back across the floodplain is not considered at present. Thus the proposed GIUS provides a lower bound on the fastest time scale for sediment to transport from different parts of the basin to the outlet. This is in contrast to the prodigious research on sediment pulses in rivers, where an emplaced pulse of sediment exceeds transport capacity and largely disperses in place [Lisle *et al.*, 1997, 2001; Cui *et al.*, 2003a, 2003b; Cui and Parker, 2005; Lisle, 2008; Sklar *et al.*, 2009].

This section includes a description of the GIUS of the Minnesota River Basin, an evaluation of its robustness to model parameter uncertainty, and a diagnostics/validation analysis of the GIUS for sand using suspended-sediment data.

5.1. Description of the GIUS

The pathway distance from each link to the outlet was grouped into seven bins to show the correspondence between the river network of the Minnesota River Basin and its WF (Figures 4a and 4b). The first two contributions to the WF (corresponding to areas at distances 0–100 and 101–200 km from the outlet in Figures 4a and 4b) are small which is reflected in the narrow width of the Minnesota River Basin near the outlet. The two peaks of the WF (corresponding to areas at distances 301–400 and 501–600 km from the outlet in Figures 4a and 4b) reflect the widest regions of the Minnesota River Basin and result from the structure of the network, where many links are within these distances from the outlet.

The WF generated using 100 bins maintains the large-scale structure of the 7-bin WF but now conveys smaller-scale information on the network structure (Figure 4c). Three distinct regions of the WF emerge: a narrow region (between normalized distance 0 and 0.3), a central region (between normalized distance 0.3 and 0.7), and a distant region (between normalized distance 0.7 and 1; Figure 4c). Each region reflects

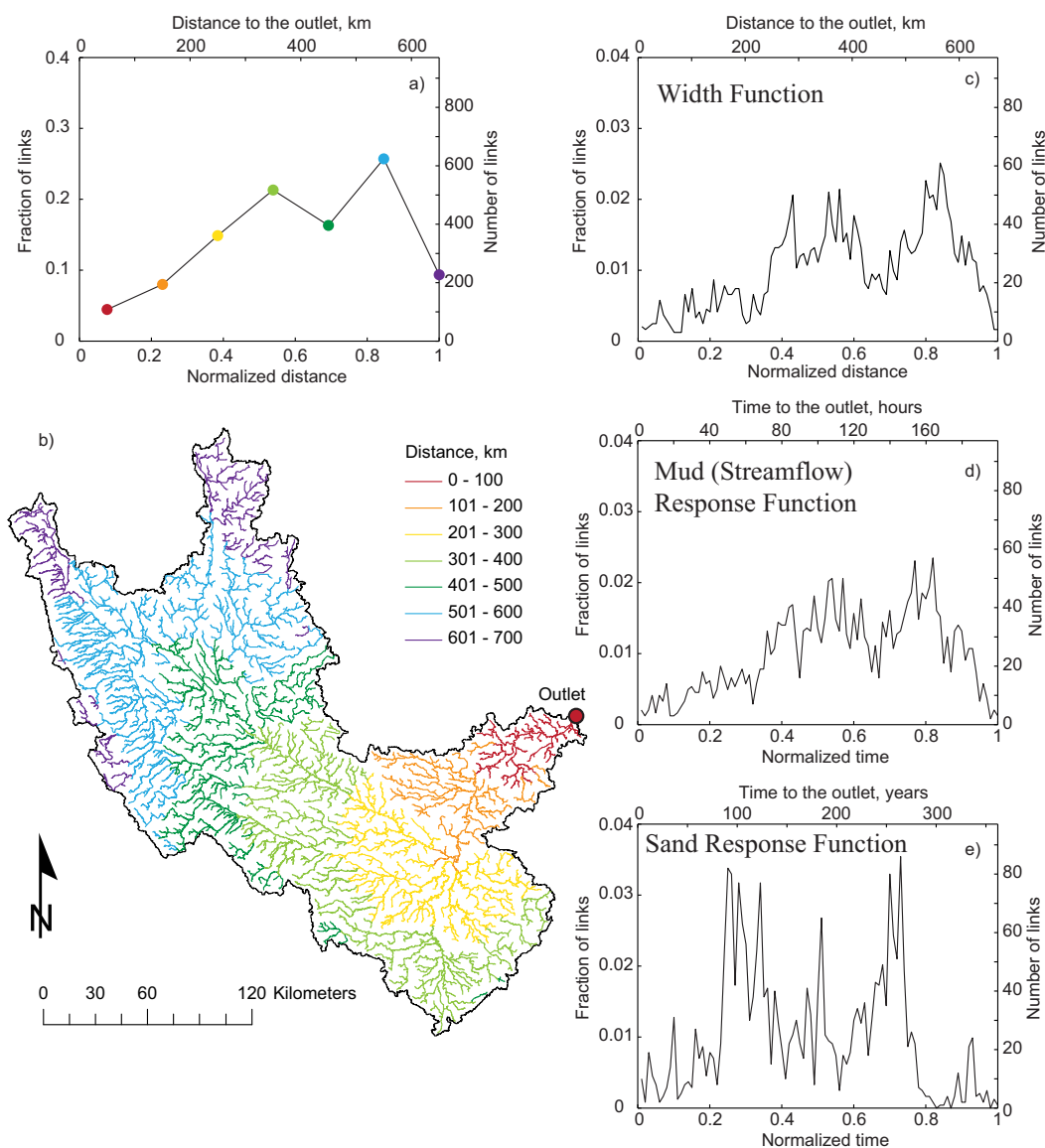


Figure 4. Width function and process-scaled width functions of the Minnesota River Basin. (a) Width function within seven discretized distance bands of the Minnesota River Basin corresponding to the (b) map of distances from each link to the outlet. (c) Width function within 100 discretized distance bands showing more fine-scale detail. (d) Process-scaled width function or geomorphic instantaneous unit sedimentograph for mud (streamflow). Note the time scale is on the order of hours to days. (e) Process-scaled width function or geomorphic instantaneous unit sedimentograph for sand (0.4 mm). Note the time scale is on the order of tens to hundreds of years.

contributions from different areas of the Minnesota River Basin. The PSWF or GIUS can be thought of as a WF generated from a network of pathway travel times rather than from a network of pathway distances. In this way, scaling link lengths by a characteristic velocity transforms the pathway-distance network nonuniformly into a pathway travel time network.

The GIUS for mud (streamflow; Figure 4d) is similar in shape to the WF because the characteristic velocity for mud transport (streamflow velocity) weakly increases with drainage area (to the 0.07 power; equation (31)). If the characteristic velocity for mud transport was a constant throughout the basin, then the GIUS would be a linearly scaled version of the width function. However, because the characteristic velocity increases downstream, the pathway travel time network is similar to the pathway-distance network except for proportionally longer upstream links and shorter downstream links. The nonlinear scaling increases the delay of contributions from upstream links and decreases the delay from downstream links compared to

the WF. The scaling of the GIUS for mud spreads out the link contributions which slightly reduces the peaks of the GIUS for mud compared to the WF.

The GIUS for sand (Figure 4e) is substantially different from the WF with peaks concentrated at a normalized distance of 0.3 and 0.7. Substituting the scaling relation for the channel slope, obtained from the 30 m DEM as

$$S_i = (0.30) A_i^{-0.31}, \tag{37}$$

into equation (33), simplifies the characteristic velocity for sand transport as a constant times the drainage area to the -0.18 power,

$$u_{s,i} = 0.05 A_i^{-0.18}. \tag{38}$$

Therefore, the characteristic velocity generally decreases downstream resulting in a pathway travel time network with proportionally shorter upstream links (decreased delay of contributions) and longer downstream links (increased delay of contributions) compared to the pathway-distance network. Contributions from upstream links more quickly enter downstream links, which concentrate the contributions from upstream links and increase the peaks of the GIUS for sand compared to the WF. The structure of the sand response truly arises from the network topology, channel slopes, and sand-transport formulation.

5.2. Robustness and Validation of the GIUS for Sand

The timing of the GIUS for sand is highly sensitive to three parameters (D_i , θ_i , and $l_{f,s}$) which appear as linear multipliers in equation (19) and therefore uniformly shift the timing of the overall response, without however affecting the shape of the response. The GIUS for sand has been computed using the D50 sand size of $D_i = 0.4$ mm from riverbed material within the Minnesota River Basin (Figure 4e) [U.S. Geological Survey, 2013]. If instead the sand has a different median size, e.g., $D_i = 0.3$ or 0.5 mm, the timing of the response function changes such that, rather than obtaining peaks at 90 and 265 years ($D_i = 0.4$ mm), the peaks would occur at 70 and 200 years ($D_i = 0.3$ mm) or 115 and 330 years ($D_i = 0.5$ mm). Thus, there is an uncertainty in the timing of the peaks of the GIUS due to uncertainty in the choice of D_i , θ_i , and $l_{f,s}$.

The shape of the GIUS for sand is only affected through the exponents on the upstream drainage area A_i and slope S_i (see equations (19) and (33)) that contribute to the transport time in a nonlinear way to rearrange contributions to the GIUS for sand (Figure 5). The exponent of the upstream drainage area was varied from 0 to 0.5 and the exponent of slope was varied from 0 to 5/2 (Figure 5). Note that the exponents of zero correspond to the width function (Figure 5m; $A^0 S^0$), which for different parameters, resulting from the specific transport dynamics, stretches to become the sand response function (Figure 5g; $A^{0.285} S^{3/2}$). Increasing the exponent on the upstream drainage area tends to smooth out the contributions to the response, whereas increasing the exponent on slope tends to concentrate contributions into peaks. For most of the variations in the exponents of the sand response function, the two peaks in the GIUS remain, although shifted, suggesting that bimodality is a relatively robust property of the GIUS for sand for the Minnesota River Basin.

As an attempt to validate the formulation of the GIUS for sand, the best estimate of the rate of total sand transport at the 2 year flow Q_2 (observed; Appendix C, approximately 120% of the rate of measured suspended-sand transport at the Q_2) was compared to the simulated rate of total sand transport at the Q_2 (simulated; Figure 6) computed as

$$Q_{s,i} = \frac{0.05}{g^{1/2} R_i^2 D_i} u_{w,i}^2 H_i^{3/2} B_i S_i^{3/2}. \tag{39}$$

A few measurements show good agreement between the simulated and observed rates of total sand transport; however, most simulated rates are an order of magnitude larger than the observed rates (Figure 6). When comparing the relative differences between the simulated and observed transport rates with the upstream drainage area (Figure 6b), the best agreement occurs at sites with large drainage areas and at a

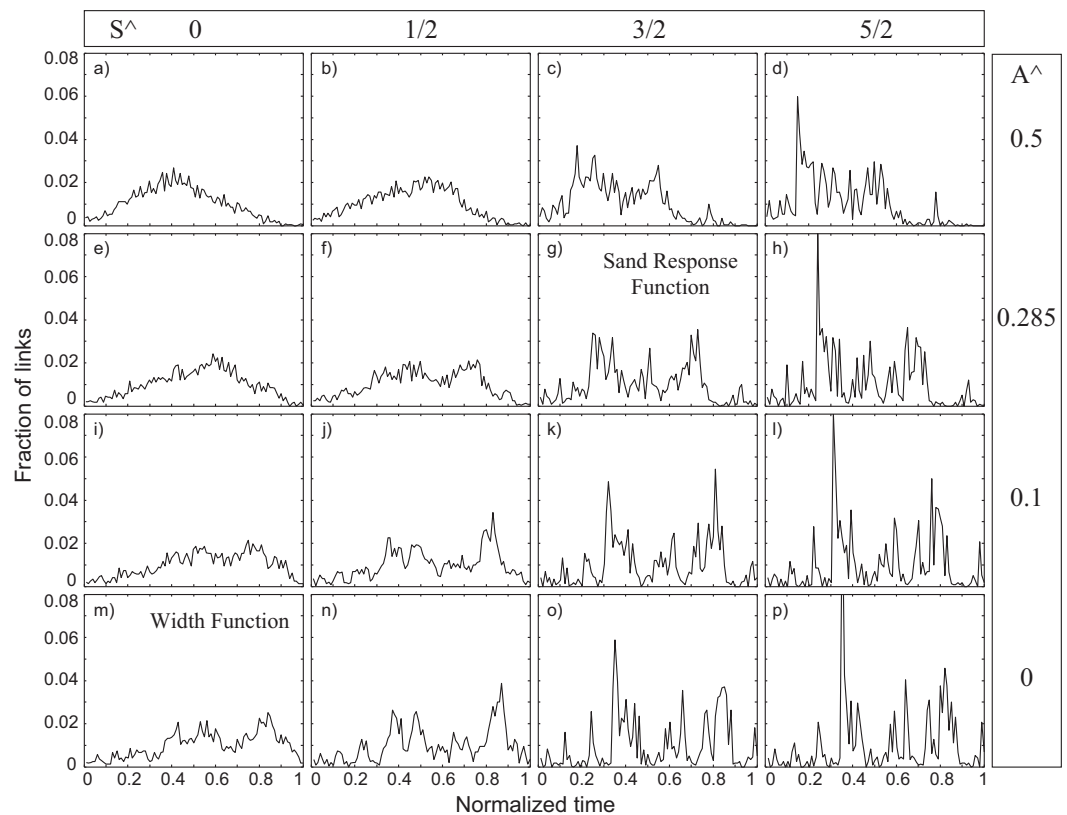


Figure 5. Sensitivity of the shape of the sand response function (geomorphologic instantaneous unit sedimentograph, GIUS). The sand response function arises from a characteristic velocity scaling $\sim A^{0.285} S^{3/2}$ (Figure 5g; see equation (33)) due to the exponents on upstream drainage area and slope that rearrange contributions to the GIUS for sand compared to the width function (Figure 5m; $A^0 S^0$). The exponent of upstream drainage area was varied from 0 to 0.5 (increases vertically) and the exponent of slope was varied from 0 to 5/2 (increases horizontally). Note that for most of the variations in exponents around the sand response function (Figure 5m) the two peaks in the GIUS remain, although shifted, suggesting that this is a relatively robust property of the GIUS for sand for the Minnesota River Basin.

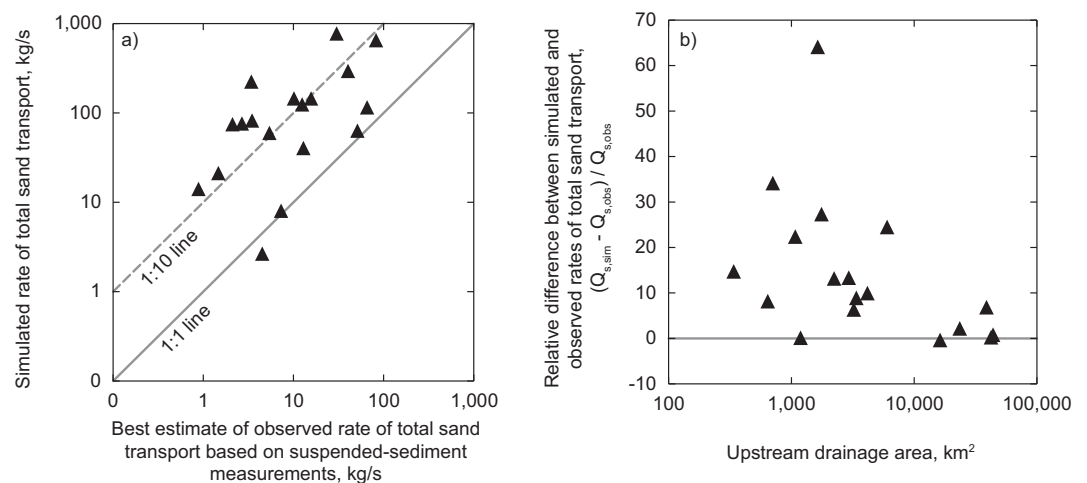


Figure 6. Comparison of the observed to simulated rates of total sand transport. (a) The best estimate of the rate of total sand transport at the Q_2 (observed; see Appendix C, approximately 120% of the measured rate of suspended-sand transport at the Q_2) was compared to the simulated rate of total sand transport at the Q_2 (simulated; see equation (39)). (b) Relative difference between simulated and observed rates of total sand transport compared to upstream drainage area. Note that the simulated rate of total sand transport represents at-capacity transport, independent of sediment supply, whereas the observations take into account spatially variable sediment supply as well as transport-limited behavior in the system. Likely this comparison identifies supply-limited (large discrepancy) versus transport-limited (small discrepancy) parts of the basin.

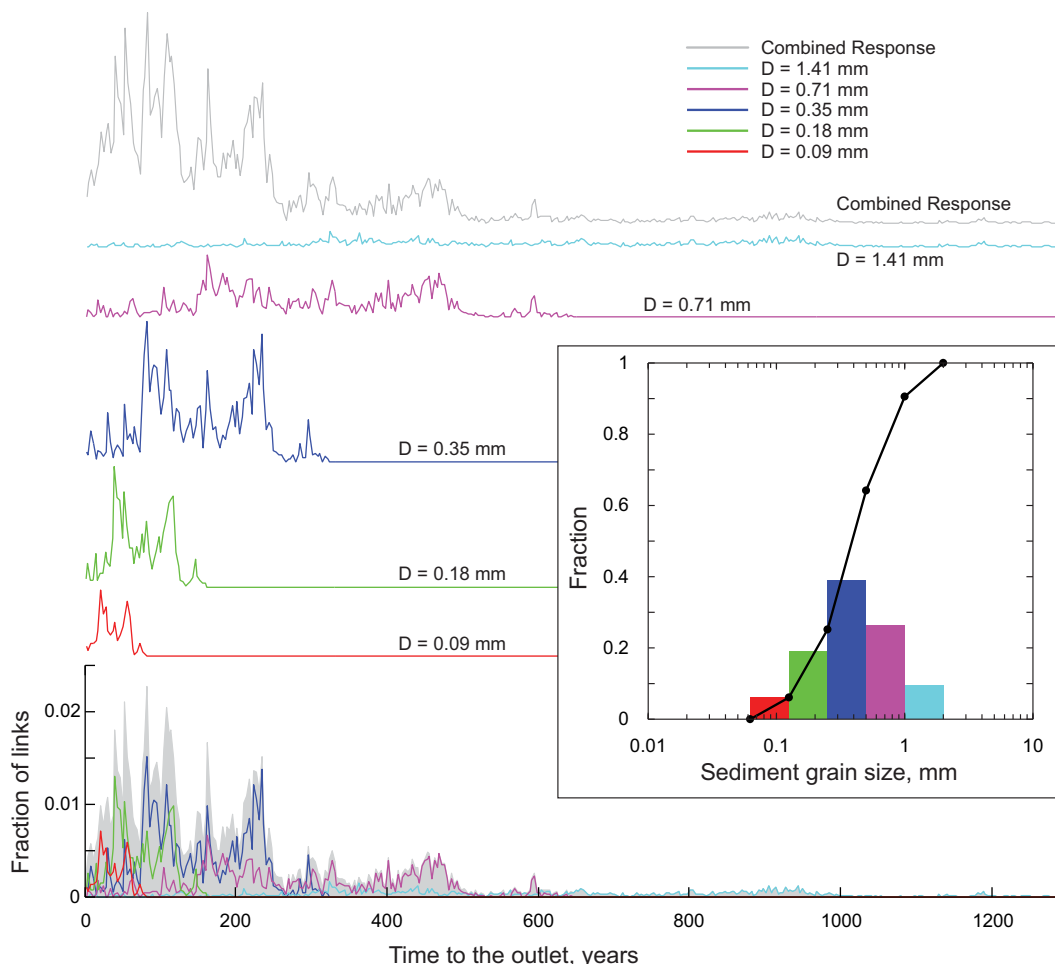


Figure 7. The geomorphologic instantaneous unit sedimentograph (GIUS) for the grain-size distribution of sand on the riverbed within the Minnesota River Basin (see inset for grain-size distribution). The GIUS for the sand distribution was generated for each individual size, scaled according to relative abundance in the grain-size distribution, and then added together across sizes to obtain the combined response. Individual size responses and the combined response are offset vertically for ease of comparison. Note that the combined response reflects the GIUS for the mode of the grain-size distribution.

few sites with small drainage areas. Note that the simulated $Q_{s,i}$ represents at-capacity transport whereas the observations take into account the actual sediment supply. It is possible that the large discrepancy between rates indicates that the transport formula or parameters used in the transport formula are not appropriate, but we suggest that this comparison may identify supply-limited versus transport-limited parts of the basin. Some upstream parts of the basin might be supply limited (simulated sand-transport capacity \gg observed transport), and at downstream links, homogenization of spatial and temporal variability may take place leading to transport-limited conditions (simulated sand-transport capacity = observed transport), which might indicate a potential for storage as any sediment supplied above capacity would go into storage. Nonetheless, where sediment supply may not be a limiting factor, there is relatively good agreement (within an order of magnitude) between the simulated and observed rates of total sand transport.

6. Partitioning Contributions to the Sedimentological Response

The GIUS is a system property and represents the response of the system to a spatially uniform input of sediment. Typically, the sediment input in such a large basin would vary spatially and temporally and this would require convolving partitioned and scaled versions of the GIUS to realize the observed sedimentological response at the outlet of the basin. We illustrate how the GIUS can be partitioned and scaled into a

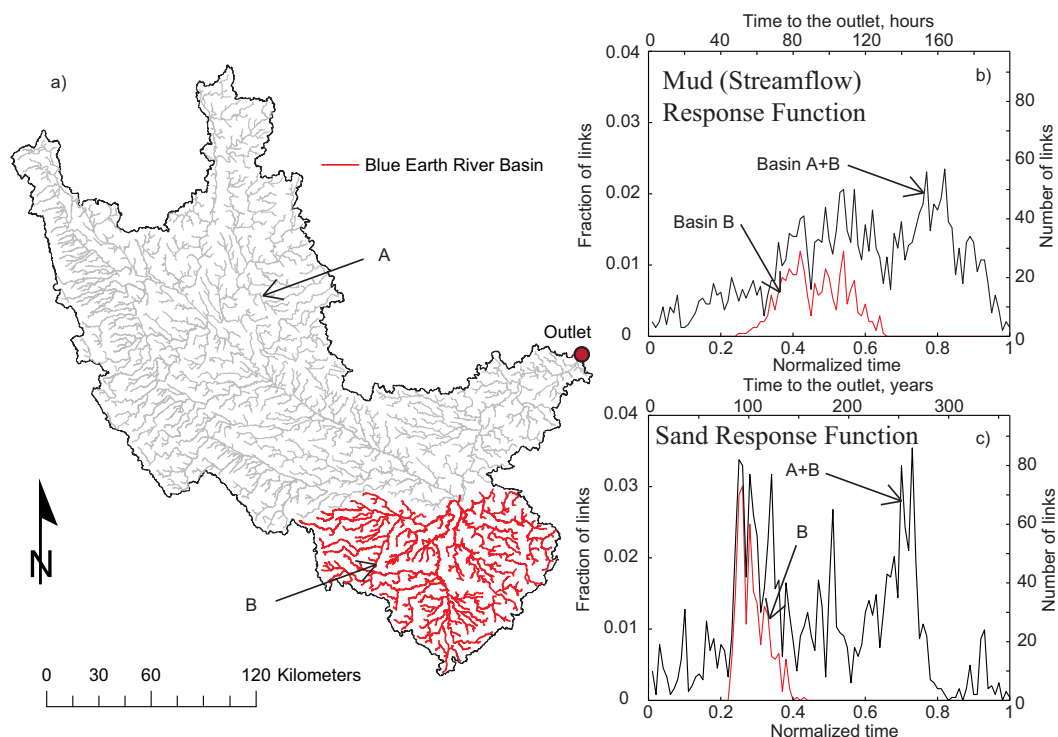


Figure 8. Partitioning contributions to the sedimentological response highlights critical sediment source areas. (a) The partition of the Blue Earth River Basin (B; red) and the rest of the basin (A; gray). (b) Sedimentological response for mud for the entire basin (A+B; black) and for the Blue Earth River Basin (B; red). (c) Sedimentological response for sand (0.4 mm) for the entire basin (A+B; black) and for the Blue Earth River Basin (B; red).

sedimentological response by considering a mixture of sediment and contributions from subbasins of the Minnesota River Basin.

The GIUS is specified for a specific grain size, such as the D50 sediment size, but in reality a mixture of sediment sizes is transported concurrently by the river network. Considering the grain-size distribution of sand on the riverbed within the Minnesota River Basin (inset Figure 7; [U.S. Geological Survey, 2013]), a GIUS for sand can be generated for each individual size, scaled according to relative abundance in the grain-size distribution, and then added together across sizes to obtain the combined response (Figure 7). Under the assumption that individual grain-size fractions sort during transport such that the transport of each fraction can be simply treated individually as a response and added together to obtain the combined response (which may not be accurate due to hiding effects [Wilcock and Crowe, 2003]), the combined response reflects the GIUS for the mode of the grain-size distribution.

The framework developed herein allows partitioning of the contributions to the GIUS based on any attributes of the geomorphic state, e.g., different subbasins which might have distinct features or sediment contributions. The Minnesota River Basin was partitioned here into two subbasins: the Blue Earth River Basin and the rest of the basin to disentangle the contribution of each to the GIUS at the outlet of the basin (Figure 8). During 2002–2006, the Blue Earth River Basin contributed over 50% of the sediment supply to the Minnesota River Basin despite the fact that it only accounts for roughly 20% of the total area [Wilcock, 2009]. Therefore, sediment contributions from the Blue Earth River Basin to the GIUS are expected to be larger than from other areas of the Minnesota River Basin. It is seen from Figure 8b that the partitioned contribution from the Blue Earth River Basin to the GIUS for mud corresponds to the central region of the response between normalized distance 0.3 and 0.7. The partitioned contribution from the Blue Earth River Basin to the GIUS for sand concentrates into the first peak at a normalized distance of 0.3 (Figure 8c). It is important to note that scaling of the network topology based on the sand-transport process has shifted the contribution of the Blue Earth River Basin from the central region of the WF to the first peak of the GIUS for sand. This highlights that nonlinear spatial stretching of the network topology based on the sediment-transport process rearranges contributions to the GIUS in unexpected ways compared to the contributions to the WF.

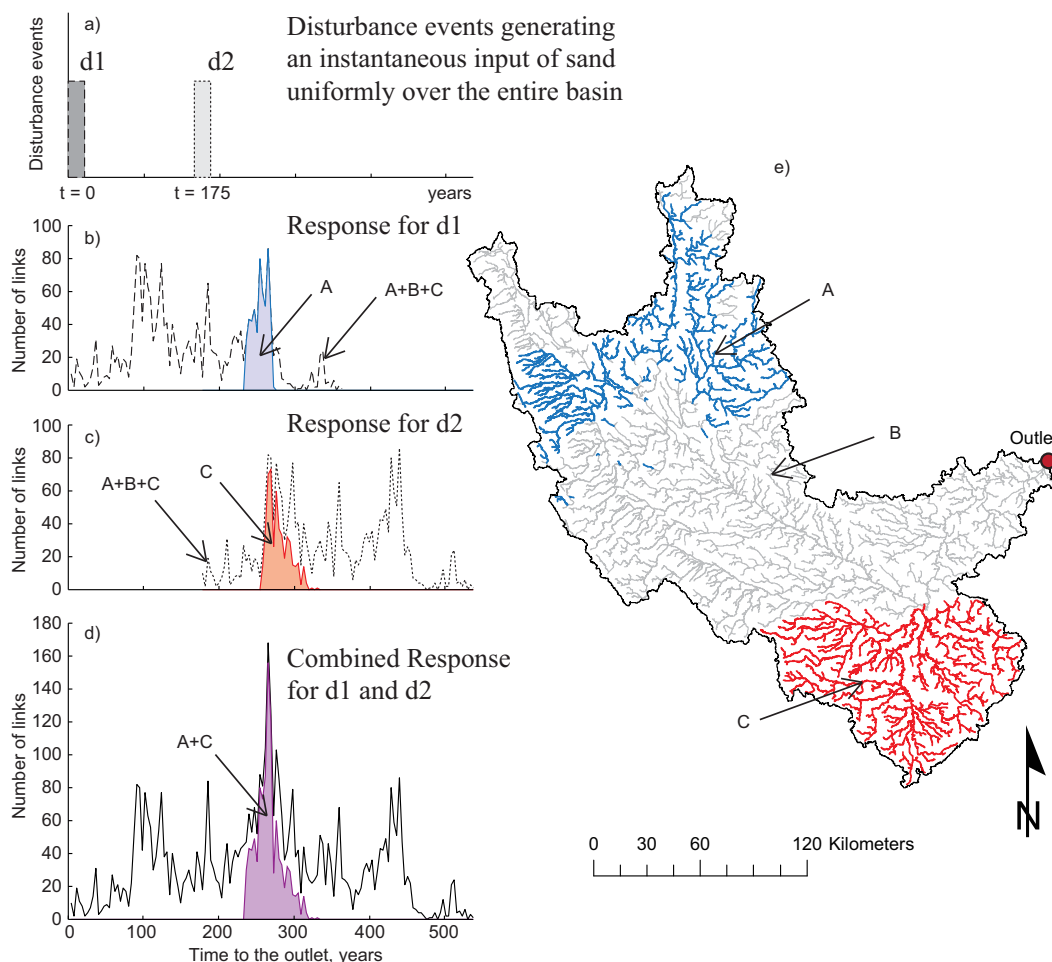


Figure 9. Synchronization of sediment fluxes can lead to amplification of the response for the Minnesota River Basin. (a) Disturbance of the landscape leading to two instantaneous inputs of sand (0.4 mm; uniformly over the basin) at 0 years (disturbance 1 or d1) and 175 years (disturbance 2 or d2). (b) Sedimentological response corresponding to d1; entire basin response (dashed line; basins A+B+C in Figure 9e) and region corresponding to the second peak of the sand response (blue shaded area; basin A in Figure 9e). (c) Sedimentological response corresponding to d2; entire basin response (dotted line; basins A+B+C in Figure 9e) and Blue Earth River Basin (red shaded area; basin C in Figure 9e). (d) Superimposed response for sand (sum of Figures 9b and 9c) into an observed response (black line) resulting in amplification of the effects of the sediment inputs. Amplification can also occur if only the regions contributing to the peaks of the response (basin A in Figure 9b and basin C in Figure 9c) are disturbed and responses superimposed (purple shaded area; A+C). (e) Partition of the basin into three regions: the region corresponding to the first peak of the sand response (red; C, Blue Earth River Basin), second peak of the sand response (blue; A), and the rest of the basin (gray; B).

7. Amplification of the Sedimentological Response

As demonstrated in the previous sections, the shape of the GIUS of a basin carries the signature not only of the river network topology but also of the specific hydraulic and stream morphologic characteristics of the channels. As a result, the peak contributions at the outlet of a basin arise from the superposition of inputs that arrive at the outlet from disparate, and even unconnected, parts of the basin. Given the long response times of sediment transport in rivers, which may be of the order of hundreds or thousands of years, one could envision changes occurring in parts of the basin at decadal or longer time scales and the associated response progressing downstream and superimposing on past responses in such a way that leads to unexpected amplifications. In this section, we demonstrate this idea using the Minnesota River Basin and its sedimentological response for sand.

Suppose a landscape disturbance event occurs which delivers an instantaneous input of sand (0.4 mm) uniformly over the entire basin at a time $t = 0$ years (d1; Figure 9a). Such an event may be extreme precipitation, which detaches sediment and the resulting overland flow entrains and delivers this sediment directly to the river network. This was likely a common mechanism during the late 19th century and early 20th

century when agricultural practices largely disturbed the landscape and left the top soil exposed and vulnerable to erosion. Extreme precipitation may also lead to very high streamflow capable of eroding and recruiting bank material into the channel. This is likely the most common mechanism today for delivering sand to the river network as soil-conservation practices have greatly improved and underground tile drainage has expanded [Belmont *et al.*, 2011].

The sedimentological response at the outlet of a basin for the disturbance event at $t = 0$ years (d1) is the GIUS for sand for the Minnesota River Basin (dashed line; Figure 9b). It is seen that the structure of the GIUS exhibits two peaks which arise from the network topology, channel slopes, and sand-transport formulation. The two prominent peaks suggest that there is a resonant frequency of sediment supply that would lead to an amplification of the response. Given regularly occurring sediment-transporting flows/events, two peaks are manifested in the response at 90 and 265 years (Figure 9b). If another landscape disturbance event occurs 175 years after the first which delivers an instantaneous input of sand (0.4 mm) uniformly over the entire basin at a time $t = 175$ years (d2; Figure 9a), the additional contribution to the sedimentological response will be similar to the first but shifted in time (Figure 9c). This assumes that disturbance events (or events that deliver sediment) are less frequent than those that transport the sediment through the river network [Lane *et al.*, 2008]. The observed response at the outlet of the basin (Figure 9d) is the superposition of the individual responses (Figures 9b and 9c) leading to an amplified sedimentological response, with a greatly increased peak at 265 years and a relatively long duration of high contributions from 250 to 280 years after the initial disturbance (Figure 9d). Conceptually, this suggests a 175 year resonance time (resonant frequency with a period of 175 years) for sand (0.4 mm) for the Minnesota River Basin.

While the GIUS conceptualizes the sedimentological response to a uniformly distributed disturbance and input to the river network, in reality these disturbances are more localized within the basin. Amplification of the sedimentological response can still occur if only specific source areas are disturbed instead of the entire landscape. For instance, if the first disturbance event (d1; Figure 9a) only disturbed a northwest region of the basin (A; Figure 9e) the sedimentological response would be only a portion (the second peak) of the GIUS (blue shaded area; Figure 9b). If the second disturbance event (d2; Figure 9a) only disturbed the Blue Earth River Basin (C; Figure 9e) the sedimentological response would be only the portion (the first peak) of the GIUS (red shaded area; Figure 9c). These seemingly isolated disturbances (in both space and time), would be ordered, delayed, and superimposed into an observed and unexpectedly amplified sedimentological response at the outlet of the basin (purple shaded area; Figure 9d).

When amplification of the sedimentological response occurs, likely there is an interaction between the two peaks that is not simply the sum of the two peaks. If the increased sediment supply to a channel is below the transport capacity, then the supply is transported downstream without a change in channel characteristics (change in channel slope or width). However, if the increased sediment supply overwhelms the transport capacity, which is likely the case, then the channel will aggrade and the change in channel characteristics will act to filter and reduce the peak of the increased sediment supply. Detailed process-based, reach-scale, sediment-transport models are best suited to quantify the specifics of the reach-scale changes due to increased sediment supply. However, this conceptual framework complements detailed process-based approaches by illuminating how inputs of sediment to the river system are structured by the river network and delayed in time due to the sediment-transport process.

The amplification of the sedimentological response could result in greater than expected aggradation of the bed of the river leading to disruption in ecosystem function, increased flood risk, and increased cost associated with remediation. Therefore, the proposed framework has identified an important vulnerability of the Minnesota River Basin to spatial and temporal changes in the basin and suggests that aggregated effects need to be seen within a whole-network framework and not in isolation.

8. Concluding Remarks

In this paper, we presented a connectivity-based conceptual framework of environmental response, focusing on the sedimentological response for mud, sand, and gravel. The proposed framework relies on performing a nonlinear process-based scaling of the network geometry (link lengths) to convert the network width function into a time response function or process-scaled width function (PSWF) where the process of interest is sediment transport. The process-scaled width function for sediment is the geomorphologic

instantaneous unit sedimentograph (GIUS) or the sedimentological response of a basin to an instantaneous unit volume of sediment uniformly entering all links of the network. The proposed framework was applied to the Minnesota River Basin to aid in understanding its long-term sedimentological response to spatially and temporally varying changes in the landscape.

It was shown that the network topology and sediment-transport dynamics in the Minnesota River Basin combine to produce a double peaked response function for sand, suggesting that there exists a resonant frequency of sediment supply that could lead to an unexpected downstream amplification of sedimentological response. The two peaks of the sand response function can be attributed to specific areas of the basin, highlighting that the disturbance of one region followed by the disturbance of another region after a certain period of time, may result in an amplification of the effects of the sediment inputs that is otherwise difficult to predict with mechanistic short-time horizon models. The synchronization and amplification of sediment delivery in specific places of a basin may result in greater than expected aggradation of the riverbed triggering disruption in ecosystem functioning, and leading to increased flood risk and increased cost associated with remediation. Therefore, the proposed framework has identified an important vulnerability of the Minnesota River Basin to spatial and temporal structuring of sediment delivery, and can aid in understanding how climatic trends and current and future management decisions may be unexpectedly superimposed on this landscape as it undergoes intensive human management while it is still adjusting to past geologic disturbances.

Appendix A: Hydraulic Geometry Scaling

Hydraulic geometry scaling was based on field measurements from 23 USGS streamflow-gaging stations in the Minnesota River Basin (see Figure 2 for gage locations) [U.S. Geological Survey, 2013]. A representative bankfull flow at each gage was determined from a frequency analysis of annual peak flows, where bankfull flow was chosen as the 2 year recurrence interval peak flow (Q_2 or 2 year flow [$L^3 T^{-1}$]) and determined as the daily streamflow that has a 50% chance of being exceeded in any year. Then the hydraulic characteristics ($u_{w,i}$ [$L T^{-1}$], H_i [L], and B_i [L]) at the Q_2 at each gage were obtained by regressing the measured hydraulic characteristics made during USGS streamflow measurements against streamflow, and taking the values of the hydraulic characteristics at the Q_2 (figures not shown). Downstream hydraulic geometry relations were developed by regressing the Q_2 with each hydraulic characteristic obtained at each gage for all 23 gages in the basin (Figures A1a–A1c).

The downstream hydraulic geometry relations for the Minnesota River Basin were obtained as:

$$B_i = (5.34)Q_{2,i}^{0.48}, \tag{A1}$$

$$H_i = (0.321)Q_{2,i}^{0.42}, \tag{A2}$$

and

$$u_{w,i} = (0.583)Q_{2,i}^{0.10}, \tag{A3}$$

where $Q_{2,i}$ is specified in m^3/s , B_i in m , H_i in m , and $u_{w,i}$ in m/s . Typical exponents for these relations are 0.50, 0.40, and 0.10 for the $B_i \sim Q_{2,i}$, $H_i \sim Q_{2,i}$, and $u_{w,i} \sim Q_{2,i}$ scaling relations, respectively [Leopold and Maddock, 1953; Park, 1977], which are in close agreement with those of the Minnesota River Basin. It is noted that the velocity hydraulic geometry relation has a low coefficient of determination ($R^2 = 0.12$; Figure A1c), highlighting the spatial heterogeneity in this basin which calls for a spatially explicit analysis. Additionally, the Q_2 was found to scale with upstream drainage area, A_i [L], (Figure A1d) as

$$Q_{2,i} = (1.4e-5)A_i^{0.70}, \tag{A4}$$

where A_i is specified in m^2 . Typically, this exponent is 0.75 and varies from 0.65 to 0.80 for bankfull flow [Leopold et al., 1964], which is in close agreement with that of the Minnesota River Basin.

Combining the hydraulic geometry relations of equations (A1–A3) with equation (A4) gives the scaling of hydraulic characteristics with upstream drainage area for the Minnesota River Basin as:

$$B_i = (0.024)A_i^{0.34}, \tag{A5}$$

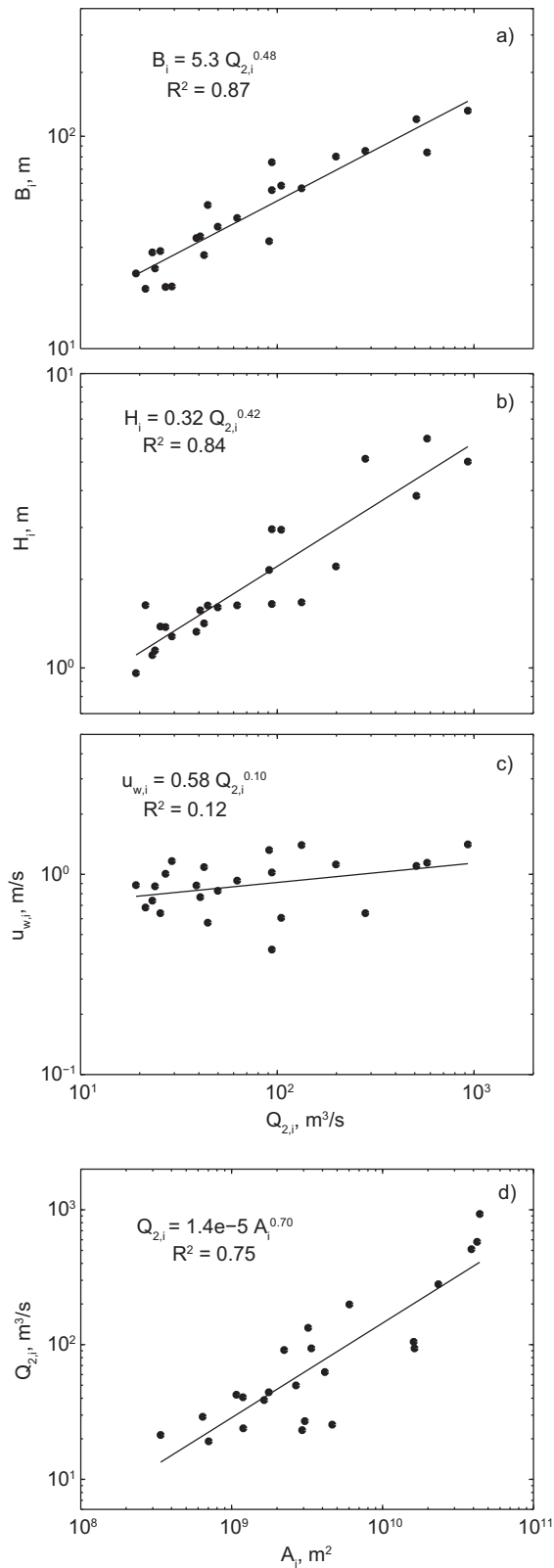


Figure A1. Hydraulic geometry scaling based on field measurements at 23 U.S. Geological Survey streamflow-gaging stations in the Minnesota River Basin (see Figure 2 for gage locations) of (a) channel width, (b) flow depth, and (c) streamflow velocity versus the 2 year recurrence interval peak flow (obtained from a frequency analysis of annual peak flows for each station). (d) Scaling of the 2 year recurrence interval peak flow versus drainage area.

$$H_i = (0.0029)A_i^{0.29}, \tag{A6}$$

and

$$u_{w,i} = (0.20)A_i^{0.07}, \tag{A7}$$

where A_i is specified in m^2 , B_i in m, H_i in m, and $u_{w,i}$ in m/s.

Appendix B: Intermittency Factor for Sand Transport

The intermittency factor for sand transport for the Minnesota River Basin was calculated at USGS streamflow-gaging station 05325000, Minnesota River at Mankato, Minnesota (see Figure 2 for gage location) and assumed to apply to the entire basin. The approach for determining the intermittency factor (first introduced by Paola *et al.* [1992]) follows the approach outlined by Parker [2004].

The volumetric transport rate of sand per unit width at the Q_2 (2 year (~bankfull) flow), $q_{s,b}$ [$L^2 T^{-1}$], was computed using equations ((8), (13), (10), and (11)). Then the daily streamflow record at the Mankato gage was used to compute nonparametrically the k th-percentile daily streamflow, q_k [$L^2 T^{-1}$], and its corresponding probability of occurrence, p_k . From q_k , the volumetric transport rate of sand per unit width in the k th percentile, $q_{s,k}$ [$L^2 T^{-1}$], was then computed for all k percentiles using equations ((8), (13), (10), and (11)). Next, the mean annual volumetric transport rate of sand per unit width, \bar{q}_s [$L^2 T^{-1}$], was computed as

$$\bar{q}_s = \sum_k p_k q_{s,k}, \tag{B1}$$

by summing the product $p_k q_{s,k}$ over all k percentiles. Finally, the intermittency factor for sand transport, $I_{f,s}$, was computed as

$$I_{f,s} = \frac{\bar{q}_s}{q_{s,b}}. \tag{B2}$$

For the Minnesota River at Mankato, the intermittency factor for sand was computed as $I_{f,s} = 0.175$. This is the fraction of time per year that continuous Q_2 would yield the mean annual sand load.

Appendix C: Best Estimate of the Rate of Total Sand Transport

Estimates of the rate of total sand transport were obtained from suspended-sediment measurements at 18 USGS streamflow-gaging stations in the Minnesota River Basin (see Figure 2 for gage locations) as follows. At each gage, suspended-sediment concentration and sand fraction, if not a full grain-size distribution, was measured along with streamflow at different instants of time and flows [U.S. Geological Survey, 2013]. Suspended-sediment concentration and sand fraction at the 2 year recurrence interval peak flow (Q_2) was estimated from the measurements at each gage. For the majority of sites, approximately 30% of the measured suspended sediment was sand at the Q_2 . The rate of suspended-sand transport at the Q_2 was computed by multiplying the suspended-sediment concentration by the sand fraction and the Q_2 streamflow. The rate of total sand transport at the Q_2 was then computed following the method of Shah-Fairbank *et al.* [2011] (and using the method of Guo and Julien [2004] to compute the Einstein integrals) from the rate of suspended-sand transport at the Q_2 , bed shear stress (estimated from Q_2 and channel dimensions), suspended-sediment fall velocity (estimated using the equation of Ferguson and Church [2004] and measured D50 sand size in suspension, ~ 0.15 mm [U.S. Geological Survey, 2013]), and D65 of bed material (from bed-material measurements at gages, ~ 1 mm [U.S. Geological Survey, 2013]). In the end, this method generally estimated the rate of total sand transport at the Q_2 equal to approximately 120% of the measured rate of suspended-sand transport at the Q_2 , and represents the best estimate of the observed rate of total sand transport (including both suspended and bed load transport) at the Q_2 from suspended-sediment measurements at gages.

Notation

a_i	directly contributing area to the i th link [L^2].
A_i	drainage area upstream of the i th link [L^2].
B_i	channel width of the i th link [L].
$C_{f,i}$	friction coefficient of the i th link.
D_i	sediment grain size in the i th link [L].
g	acceleration due to gravity [$L T^{-2}$].
H_i	cross-section averaged flow depth of the i th link [L].
i	index denoting spatial location within the network.
$I_{f,g}$	intermittency factor for gravel transport.
$I_{f,s}$	intermittency factor for sand transport.
j	connectivity index along pathway γ_i .
k	index of a percentile.
ℓ_i	length of the i th link [L].
$L_{a,i}$	active layer thickness of the i th link [L].
L_i	pathway distance from geomorphic state ξ_i to the outlet [L].
L_{\max}	maximum pathway distance [L].
p_k	probability of occurrence of the k th-percentile daily streamflow.
$q_{g,i}$	volumetric transport rate of gravel through the i th link [$L^2 T^{-1}$].
$q_{g^*,i}$	dimensionless volumetric transport rate of gravel through the i th link.
q_k	k th-percentile daily streamflow [$L^2 T^{-1}$].
\bar{q}_s	mean annual volumetric transport rate of sand per unit width [$L^2 T^{-1}$].
$q_{s,b}$	volumetric transport rate of sand per unit width at the 2 year (bankfull) flow [$L^2 T^{-1}$].
$q_{s,i}$	volumetric transport rate of sand through the i th link [$L^2 T^{-1}$].
$q_{s,k}$	volumetric transport rate of sand per unit width in the k th percentile [$L^2 T^{-1}$].
$q_{s^*,i}$	dimensionless volumetric transport rate of sand through the i th link.
$Q_{g,i}$	volumetric transport rate of gravel through the i th link [$L^3 T^{-1}$].
$Q_{s,i}$	volumetric transport rate of sand through the i th link [$L^3 T^{-1}$].
$Q_{w,i}$	streamflow or volumetric transport rate of water through the i th link [$L^3 T^{-1}$].
Q_2	2 year recurrence interval peak flow [$L^3 T^{-1}$].
R_i	submerged specific gravity of sediment in the i th link.
S_i	slope of the i th link.
t	arbitrary arrival time of a particle at the outlet of a basin [T].
$t_{p,i}$	process-specific transport time through the i th link [T].
$t_{g,i}$	travel time of gravel through the i th link [T].
$t_{g,i}^f$	travel time of gravel through the i th link during constant bankfull flow [T].
$t_{s,i}$	travel time of sand through the i th link [T].
$t_{s,i}^f$	travel time of sand through the i th link during constant bankfull flow [T].
$t_{w,i}$	travel time of mud (streamflow) through the i th link [T].
$T_{p,i}$	process-specific pathway travel time from the i th link to the outlet [T].
$T_{p,\max}$	maximum process-specific pathway travel time [T].
$T_{g,i}$	pathway travel time of gravel from the i th link to the outlet [T].
$T_{s,i}$	pathway travel time of sand from the i th link to the outlet [T].
$T_{w,i}$	pathway travel time of mud (streamflow) from the i th link to the outlet [T].
$u_{p,i}$	process-specific velocity through the i th link [$L T^{-1}$].
$u_{g,i}$	characteristic velocity of gravel in the i th link [$L T^{-1}$].
$u_{s,i}$	characteristic velocity of sand in the i th link [$L T^{-1}$].
$u_{w,i}$	characteristic velocity of the flow in the i th link [$L T^{-1}$].
$W(x)$	width function.
$W_p(t)$	process-scaled width function.
$W_g(t)$	process-scaled width function for gravel transport.
$W_s(t)$	process-scaled width function for sand transport.
$W_w(t)$	process-scaled width function for mud transport (streamflow).

x	arbitrary pathway distance from the outlet measured along the network [L].
α_g	coefficient of the gravel-transport formula.
α_{HA}	coefficient of the $H_i \sim A_i$ scaling relation.
$\alpha_{u_w A}$	coefficient of the $u_{w,i} \sim A_i$ scaling relation.
β_g	exponent of the gravel-transport formula.
β_{HA}	exponent of the $H_i \sim A_i$ scaling relation.
$\beta_{u_w A}$	exponent of the $u_{w,i} \sim A_i$ scaling relation.
γ_i	connectivity of geomorphic state ζ_i to the outlet.
θ_i	scale factor for determining the characteristic vertical length scale for sand transport.
$\zeta_{f,i}$	geomorphic fluvial state of the i th link.
ζ_i	geomorphic state of the i th link.
ρ	density of water [$M L^{-3}$].
$\tau_{b,i}$	bed shear stress in the i th link [$M L^{-1} T^{-2}$].
$\tau_{*c,i}$	critical dimensionless bed shear stress for the initiation of motion in the i th link.
$\tau_{*,i}$	dimensionless bed shear stress in the i th link.
Ω	index of the basin outlet.

Acknowledgments

This research was funded by NSF grant EAR-1209402 under the Water Sustainability and Climate Program. The first author acknowledges the support of a UMN Civil Engineering departmental fellowship and the second author acknowledges the support of the Joseph T. and Rose S. Ling Endowed Professorship. We sincerely thank Jim Pizzuto (Univ. of Delaware), Peter Wilcock (Johns Hopkins Univ.), and an anonymous reviewer for their insightful comments which helped improve the presentation of our work. We also thank the Editor (Graham Sander) and Associate Editor (anonymous) for an efficient and constructive review process.

References

- Belmont, P. (2011), Floodplain width adjustments in response to rapid base level fall and knickpoint migration, *Geomorphology*, *128*, 92–102, doi:10.1016/j.geomorph.2010.12.026.
- Belmont, P., et al. (2011), Large shift in source of fine sediment in the Upper Mississippi River, *Environ. Sci. Technol.*, *45*, 8804–8810, doi:10.1021/es2019109.
- Benda, L., and T. Dunne (1997a), Stochastic forcing of sediment routing and storage in channel networks, *Water Resour. Res.*, *33*, 2865–2880, doi:10.1029/97WR02387.
- Benda, L., and T. Dunne (1997b), Stochastic forcing of sediment supply to channel networks from landsliding and debris flow, *Water Resour. Res.*, *33*, 2849–2863, doi:10.1029/97WR02388.
- Bhunya, P. K., S. K. Jain, P. K. Singh, and S. K. Mishra (2010), A simple conceptual model of sediment yield, *Water Resour. Manage.*, *24*, 1697–1716, doi:10.1007/s11269-009-9520-4.
- Botter, G., E. Bertuzzo, and A. Rinaldo (2010), Transport in the hydrologic response: Travel time distributions, soil moisture dynamics, and the old water paradox, *Water Resour. Res.*, *46*, W03514, doi:10.1029/2009WR008371.
- Clayton, L., and S. R. Moran (1982), Chronology of late Wisconsinan glaciation in middle North America, *Quat. Sci. Rev.*, *1*, 55–82.
- Cui, Y., and G. Parker (2005), Numerical model of sediment pulses and sediment-supply disturbances in mountain rivers, *J. Hydraul. Eng.*, *131*(8), 646–656, doi:10.1061/(ASCE)0733-9429(2005)131:8(646).
- Cui, Y., G. Parker, T. E. Lisle, J. Gott, M. E. Hansler-Ball, J. E. Pizzuto, N. E. Allmendinger, and J. M. Reed (2003a), Sediment pulses in mountain rivers: 1. Experiments, *Water Resour. Res.*, *39*(9), 1239, doi:10.1029/2002WR001803.
- Cui, Y., G. Parker, J. Pizzuto, and T. E. Lisle (2003b), Sediment pulses in mountain rivers: 2. Comparison between experiments and numerical predictions, *Water Resour. Res.*, *39*(9), 1240, doi:10.1029/2002WR001805.
- Dooge, J. C. I. (1973), Linear theory of hydrologic systems, *Tech. Bull. 1468, EGU Reprint Ser. 1*, 327 p., Agric. Res. Serv., U.S. Dep. of Agric., Eur. Geosci. Union, Katlenburg-Lindau, Germany.
- Engelund, F., and E. Hansen (1967), *A Monograph on Sediment Transport in Alluvial Streams*, 62 p., Tek. Forlag, Copenhagen, Denmark.
- Ferguson, R. I., and M. Church (2004), A simple universal equation for grain settling velocity, *J. Sediment. Res.*, *74*(6), 933–937, doi:10.1306/051204740933.
- Fryirs, K. (2013), (Dis)Connectivity in catchment sediment cascades: A fresh look at the sediment delivery problem, *Earth Surf. Processes Landforms*, *38*, 30–46, doi:10.1002/esp.3242.
- Garcia, M. H. (2008), Sediment transport and morphodynamics, in *Sedimentation Engineering: Processes, Measurements, Modeling, and Practice: ASCE Manuals and Reports on Engineering Practice*, vol. 110, edited by M. H. Garcia, pp. 21–163, Am. Soc. of Civ. Eng., Reston, Va.
- Gracia-Sanchez, J. (1996), Generation of synthetic sedimentgraphs, *Hydrol. Processes*, *10*(9), 1181–1191, doi:10.1002/(SICI)1099-1085(199609)10:9<1181::AID-HYP369>3.0.CO;2-X.
- Gran, K. B., P. Belmont, S. S. Day, C. Jennings, A. Johnson, L. Perg, and P. R. Wilcock (2009), Geomorphic evolution of the Le Sueur River, Minnesota, USA, and implications for current sediment loading, in *Management and Restoration of Fluvial Systems with Broad Historical Changes and Human Impacts*, vol. 451, edited by L. A. James, S. L. Rathburn, and G. R. Whittecar, pp. 119–130, Geol. Soc. of Am., Boulder, Colo., doi:10.1130/2009.2451(08).
- Gran, K. B., P. Belmont, S. S. Day, N. Finnegan, C. Jennings, J. W. Lauer, and P. R. Wilcock (2011), Landscape evolution in south-central Minnesota and the role of geomorphic history on modern erosional processes, *GSA Today*, *21*(9), 7–9, doi:10.1130/G121A.1.
- Guo, J., and P. Y. Julien (2004), Efficient algorithm for computing Einstein integrals, *J. Hydraul. Eng.*, *130*(12), 1198–1201, doi:10.1061/(ASCE)0733-9429(2004)130:12(1198).
- Gupta, V. K., and O. J. Mesa (1988), Runoff generation and hydrologic response via channel network geomorphology—Recent progress and open problems, *J. Hydrol.*, *102*, 3–28, doi:10.1016/0022-1694(88)90089-3.
- Gupta, V. K., E. Waymire, and C. T. Wang (1980), A representation of an instantaneous unit hydrograph from geomorphology, *Water Resour. Res.*, *16*, 855–862, doi:10.1029/WR016i005p0855.
- Gupta, V. K., E. Waymire, and I. Rodriguez-Iturbe (1986), On scales, gravity and network structure in basin runoff, in *Scale Problems in Hydrology*, edited by V. K. Gupta, I. Rodriguez-Iturbe, and E. F. Wood, pp. 159–184, D. Reidel, Dordrecht, Holland.
- Harvey, A. M. (2002), Effective timescales of coupling within fluvial systems, *Geomorphology*, *44*, 175–201, doi:10.1016/S0169-555X(01)00174-X.

- Johnson, J. W. (1943), Distribution graphs of suspended-matter concentration, *Trans. Am. Soc. Civ. Eng.*, 108(1), 941–956.
- Kalin, L., R. S. Govindaraju, and M. M. Hantush (2004a), Development and application of a methodology for sediment source identification. I: Modified unit sedimentograph approach, *J. Hydrol. Eng.*, 9(3), 184–193, doi:10.1061/(ASCE)1084-0699(2004)9:3(184).
- Kalin, L., R. S. Govindaraju, and M. M. Hantush (2004b), Development and application of a methodology for sediment source identification. II: Optimization approach, *J. Hydrol. Eng.*, 9(3), 194–207, doi:10.1061/(ASCE)1084-0699(2004)9:3(194).
- Kelley, D. W., and E. A. Nater (2000), Historical sediment flux from three watersheds into Lake Pepin, Minnesota, USA, *J. Environ. Qual.*, 29, 561–568, doi:10.2134/jeq2000.00472425002900020025x.
- Kirkby, M. J. (1976), Tests of the random network model and its application to basin hydrology, *Earth Surf. Processes*, 1, 197–212, doi:10.1002/esp.3290010302.
- Kumar, S., and R. A. Rastogi (1987), A conceptual catchment model for estimating suspended sediment flow, *J. Hydrol.*, 95, 155–163, doi:10.1016/0022-1694(87)90122-3.
- Lane, S. N., S. C. Reid, V. Tayefi, D. Yu, and R. J. Hardy (2008), Reconceptualising coarse sediment delivery problems in rivers as catchment-scale and diffuse, *Geomorphology*, 98, 227–249, doi:10.1016/j.geomorph.2006.12.028.
- Lauer, J. W., and G. Parker (2008), Net local removal of floodplain sediment by river meander migration, *Geomorphology*, 96, 123–149, doi:10.1016/j.geomorph.2007.08.003.
- Lee, K. T., and C.-C. Yang (2010), Estimation of sediment yield during storms based on soil and watershed geomorphology characteristics, *J. Hydrol.*, 382, 145–153, doi:10.1016/j.jhydrol.2009.12.025.
- Lee, Y. H., and V. P. Singh (1999), Prediction of sediment yield by coupling Kalman filter with instantaneous unit sediment graph, *Hydrol. Processes*, 13(17), 2861–2875, doi:10.1002/(SICI)1099-1085(19991215)13:17<2861::AID-HYP805>3.0.CO;2-Z.
- Leopold, L. B., and T. Maddock Jr. (1953), The hydraulic geometry of stream channels and some physiographic implications, *U.S. Geol. Surv. Prof. Pap.*, 252, 57 p.
- Leopold, L. B., M. G. Wolman, and J. P. Miller (1964), *Fluvial Processes in Geomorphology*, W. H. Freeman, San Francisco, Calif.
- Lisle, T. E. (2008), The evolution of sediment waves influenced by varying transport capacity in heterogeneous rivers, in *Gravel Bed Rivers VI: From Process Understanding to River Restoration*, edited by H. Habersack, H. Piegay, and M. Rinaldi, pp. 443–472, Elsevier, Amsterdam, doi:10.1016/S0928-2025(07)11136-6.
- Lisle, T. E., J. E. Pizzuto, H. Ikeda, F. Iseya, and Y. Kodama (1997), Evolution of a sediment wave in an experimental channel, *Water Resour. Res.*, 33, 1971–1981, doi:10.1029/97WR01180.
- Lisle, T. E., Y. Cui, G. Parker, J. E. Pizzuto, and A. M. Dodd (2001), The dominance of dispersion in the evolution of bed material waves in gravel-bed rivers, *Earth Surf. Processes Landforms*, 26, 1409–1420, doi:10.1002/esp.300.
- Maidment, D. R., F. Olivera, A. Calver, A. Eatherall, and W. Fraczek (1996), Unit hydrograph derived from a spatially distributed velocity field, *Hydrol. Processes*, 10(6), 831–844, doi:10.1002/(SICI)1099-1085(199606)10:6<831::AID-HYP374>3.0.CO;2-N.
- Malmon, D. V., T. Dunne, and S. L. Reneau (2003), Stochastic theory of particle trajectories through alluvial valley floors, *J. Geol.*, 111(5), 525–542, doi:10.1086/376764.
- Marschner, F. J. (1974), *The Original Vegetation of Minnesota, a Map Compiled in 1930 by F.J. Marschner Under the Direction of M.L. Heinselman of the United States Forest Service*, Map 1:500,000, Cartogr. Lab. of the Dep. of Geogr., Univ. of Minn., St. Paul, Minn.
- Mesa, O. J., and E. R. Miffin (1986), On the relative role of hillslope and network geometry in hydrologic response, in *Scale Problems in Hydrology*, edited by V. K. Gupta, I. Rodriguez-Iturbe, and E. F. Wood, pp. 1–17, D. Reidel, Dordrecht, Holland.
- Musser, K., S. Kudelka, and R. Moore (2009), *Minnesota River Basin trends*, water resources center report, 64 p., Minn. State Univ., Mankato, Minn. (<http://mrdbc.mnsu.edu/minnesota-river-basin-trends-report>) last accessed April 29, 2014.
- Muzik, I. (1996), Flood modeling with GIS-derived distributed unit hydrographs, *Hydrol. Processes*, 10(10), 1401–1409, doi:10.1002/(SICI)1099-1085(199610)10:10<1401::AID-HYP469>3.0.CO;2-3.
- Nash, J. E. (1957), The form of the instantaneous unit hydrograph, *Bull. Int. Assoc. Sci. Hydrol.*, 3, 114–121.
- Paola, C., P. L. Hellert, and C. L. Angevine (1992), The large-scale dynamics of grain-size variation in alluvial basins. 1: Theory, *Basin Res.*, 4(2), 73–90, doi:10.1111/j.1365-2117.1992.tb00145.x.
- Park, C. C. (1977), World-wide variations in hydraulic geometry exponents of stream channels: An analysis and some observations, *J. Hydrol.*, 33, 133–146, doi:10.1016/0022-1694(77)90103-2.
- Parker, G. (2004), 1D aggradation and degradation of rivers: Normal flow assumption, chap. 14, in *1D Sediment Transport Morphodynamics with Applications to Rivers and Turbidity Currents*, Urbana, Illinois, 38 p. [Available at http://hydrolab.illinois.edu/people/parkerg/morphodynamics_e-book.htm, last accessed 5 May 2013.]
- Parker, G. (2008), Transport of gravel and sediment mixtures, in *Sedimentation Engineering: Processes, Measurements, Modeling, and Practice: ASCE Manuals and Reports on Engineering Practice*, vol. 110, edited by M. H. Garcia, pp. 165–251, Am. Soc. of Civ. Eng., Reston, Va.
- Passalacqua, P., P. Belmont, and E. Foufoula-Georgiou (2012), Automatic geomorphic feature extraction from lidar in flat and engineered landscapes, *Water Resour. Res.*, 48, W03528, doi:10.1029/2011WR010958.
- Pizzuto, J., et al. (2014), Characteristic length scales and time-averaged transport velocities of suspended sediment in the mid-Atlantic region, USA, *Water Resour. Res.*, 50, 790–805, doi:10.1002/2013WR014485.
- Raghuwanshi, N. S., R. A. Rastogi, and S. Kumar (1994), Instantaneous-unit sediment graph, *J. Hydraul. Eng.*, 120(4), 495–503, doi:10.1061/(ASCE)0733-9429(1994)120:4(495).
- Reid, S. C., S. N. Lane, D. R. Montgomery, and C. J. Brookes (2007a), Does hydrological connectivity improve modelling of coarse sediment delivery in upland environments?, *Geomorphology*, 90, 263–282, doi:10.1016/j.geomorph.2006.10.023.
- Reid, S. C., S. N. Lane, J. M. Berney, and J. Holden (2007b), The timing and magnitude of coarse sediment transport events within an upland, temperate gravel-bed river, *Geomorphology*, 83, 152–182, doi:10.1016/j.geomorph.2006.06.030.
- Rinaldo, A., G. Botter, E. Bertuzzo, A. Uccelli, T. Settin, and M. Marani (2006a), Transport at basin scales: 1. Theoretical framework, *Hydrol. Earth Syst. Sci.*, 10, 19–29, doi:10.5194/hess-10-19-2006.
- Rinaldo, A., G. Botter, E. Bertuzzo, A. Uccelli, T. Settin, and M. Marani (2006b), Transport at basin scales: 2. Applications, *Hydrol. Earth Syst. Sci.*, 10, 31–48, doi:10.5194/hess-10-31-2006.
- Rodriguez-Iturbe, I., and A. Rinaldo (1997), *Fractal River Basins: Chance and Self-Organization*, 564 p., Cambridge Univ. Press, New York.
- Rodriguez-Iturbe, I., and J. B. Valdes (1979), The geomorphologic structure of hydrologic response, *Water Resour. Res.*, 15, 1409–1420, doi:10.1029/WR015i006p01409.
- Schottler, S. P., J. Ulrich, P. Belmont, R. Moore, J. W. Lauer, D. R. Engstrom, and J. E. Almendinger (2014), Twentieth century agricultural drainage creates more erosive rivers, *Hydrol. Processes*, 28(4), 1951–1961, doi:10.1002/hyp.9738.
- Shah-Fairbank, S. C., P. Y. Julien, and D. C. Baird (2011), Total sediment load from SEMEP using depth-integrated concentration measurements, *J. Hydraul. Eng.*, 137(12), 1606–1614, doi:10.1061/(ASCE)HY.1943-7900.0000466.

- Sharma, K. D., R. P. Dhir, and J. S. R. Murthy (1992), Modelling suspended sediment flow in arid upland basins, *Hydrol. Sci. J.*, 37(5), 481–490, doi:10.1080/02626669209492613.
- Sherman, L. K. (1932), Streamflow from rainfall by the unit-graph method, *Eng. News Rec.*, 108, 501–505.
- Singh, P. K., P. K. Bhunya, S. K. Mishra, and U. C. Chaube (2008), A sediment graph model based on SCS-CN method, *J. Hydrol.*, 349, 244–255, doi:10.1016/j.jhydrol.2007.11.004.
- Sklar, L. S., J. Fadde, J. G. Venditti, P. Nelson, M. A. Wydzga, Y. Cui, and W. E. Dietrich (2009), Translation and dispersion of sediment pulses in flume experiments simulating gravel augmentation below dams, *Water Resour. Res.*, 45, W08439, doi:10.1029/2008WR007346.
- Troutman, B. M., and M. R. Karlinger (1985), Unit hydrograph approximations assuming linear flow through topologically random channel networks, *Water Resour. Res.*, 21, 743–754, doi:10.1029/WR021i005p00743.
- U.S. Geological Survey (2012), *National Map*, U.S. Geological Survey, Reston, Va. [Available at <http://nationalmap.gov>, last accessed 9 Nov. 2012.]
- U.S. Geological Survey (2013), *USGS Water Data for Minnesota*, U.S. Geological Survey, Reston, Va. [Available at <http://waterdata.usgs.gov/mn/nwis/>, last accessed 24 May 2013.]
- Wilcock, P. (2009), *Identifying Sediment Sources in the Minnesota River Basin*, Minnesota Pollution Control Agency, report number wq-b3-43, Mankato, MN. 16 p. (<http://www.pca.state.mn.us/index.php/view-document.html?gid=8099>) last accessed April 29, 2014.
- Wilcock, P. R., and J. C. Crowe (2003), Surface-based transport model for mixed-size sediment, *J. Hydraul. Eng.*, 129(2), 120–128, doi:10.1061/(ASCE)0733-9429(2003)129:2(120).
- Williams, J. R. (1978), A sediment graph model based on instantaneous unit sediment graph, *Water Resour. Res.*, 14, 659–664, doi:10.1029/WR014i004p00659.
- Wong, M., and G. Parker (2006), Reanalysis and correction of bed-load relation of Meyer-Peter and Muller using their own database, *J. Hydraul. Eng.*, 132(11), 1159–1168, doi:10.1061/(ASCE)0733-9429(2006)132:11(1159).